ISTANBUL TECHNICAL UNIVERSITY ★ GRADUATE SCHOOL OF SCIENCE ENGINEERING AND TECHNOLOGY

CONTRIBUTION OF AIRBORNE GRAVIMETRY TO REGIONAL GEOID DETERMINATION BY LEAST SQUARES COLLOCATION

M.Sc. THESIS

Öykü Koç

Department of Geomatics Engineering

Geomatics Engineering Programme

JULY 2020

ISTANBUL TECHNICAL UNIVERSITY ★ GRADUATE SCHOOL OF SCIENCE ENGINEERING AND TECHNOLOGY

CONTRIBUTION OF AIRBORNE GRAVIMETRY TO REGIONAL GEOID DETERMINATION BY LEAST SQUARES COLLOCATION

M.Sc. THESIS

Öykü Koç
(501181638)

Department of Geomatics Engineering

Geomatics Engineering Programme

Thesis Advisor: Assoc. Prof. Dr. Bihter EROL
Co-advisor: Prof. Dr. Riccardo BARZAGHI

JULY 2020

İSTANBUL TEKNİK ÜNİVERSİTESİ ★ FEN BİLİMLERİ ENSTİTÜSÜ

HAVA GRAVİMETRESİNİN EN KÜÇÜK KARELER KOLLOKASYON YÖNTEMİ İLE BÖLGESEL GEOİT BELİRLENMESİNE KATKISI

YÜKSEK LİSANS TEZİ

Öykü Koç
(501181638)

Geomatik Mühendisliği Anabilim Dalı

Geomatik Mühendisliği Programı

Tez Danışmanı: Doç. Dr. Bihter EROL
Eş Danışman: Prof. Dr. Riccardo BARZAGHI

TEMMUZ 2020

Öykü Koç, a M.Sc. student of ITU Graduate School of Science Engineering and Technology 501181638 successfully defended the thesis entitled "CONTRIBUTION OF AIRBORNE GRAVIMETRY TO REGIONAL GEOID DETERMINATION BY LEAST SQUARES COLLOCATION", which he/she prepared after fulfilling the requirements specified in the associated legislations, before the jury whose signatures are below.

Thesis Advisor :	**Assoc. Prof. Dr. Bihter EROL** Istanbul Technical University	.....
Co-advisor :	**Prof. Dr. Riccardo BARZAGHI** Politecnico di Milano	.....
Jury Members :	**Prof. Dr. Mustafa YANALAK** Istanbul Technical University	.....
	Prof. Dr. Hayri Hakan Denli Istanbul Technical University	.....
	Prof.Dr. Uğur DOĞAN Yıldız Technical University	.....

Date of Submission : **14 June 2020**
Date of Defense : **27 July 2020**

FOREWORD

First of all, I would like to thank my supervisor, Dr. Bihter Erol, for her guidance and support during this thesis and everything in the past 3 years.

I also would like to express my gratitude to Prof. Riccardo Barzaghi for giving me a chance to be a visitor student in Politecnico di Milano to work with him on this dissertation and providing me an environment to work during the time I spent in Milan. He has been very supportive and helpful in every sense. Also, I am grateful to Politecnico di Milano Department of Civil and Environmental Engineering (PoliMi-DICA) for sharing the softwares they developed.

Additionally, I want to express my appreciation to Aristotle University of Thessaloniki Laboratory of Gravity Field Research and Applications (AUTh-GravLab) members, especially to Dr. Vassilios Grigoriadis for computing and sharing the Global Gravity Model and Residual Terrain Model components of both airborne and terrestrial gravity data. And it was an honour to be a part of PoliMi-AUTh study group.

I would like to thank Istanbul Technical University Gravity Research Group (ITU-GRG) for their helps and contributions to improve myself in physical geodesy, and the environment it has provided me for my studies at ITU. It was a great experience to be a part of this group.

I also want to thank my family for their constant support in every sense. Last but not least, I am grateful to my friends Bengü Paşaoğlu, Mustafa Serkan Işık and Feyza Fatima Sakil for being my motivational supporters.

This thesis study was supported by ITU-BAP Project with contract number: MYL-2019-42208.

July 2020 Öykü Koç

TABLE OF CONTENTS

Page

ABBREVIATIONS

AUTh : Aristotle University of Thessaloniki
BVP : Boundary Value Problem
COV : Covariance
DEM : Digital Elevation Model
DTM : Digital Terrain Model
EDV : Error Degree Variance
EGM2008 : Earth Gravitational Model 2008
ERTM2160 : Earth Residual Terrain Modelled
FFT : Fast Fourier Transformation
GBVP : Geodetic Boundary Value Problem
GGM : Global Geopotential Models
GPS : Global Positioning System
GNSS : Global Navigation Satellite System
GRAV-D : Gravity for the Redefinition of the American Vertical Datum
GSVS17 : Geoid Slope Validation Survey 2017
IAG : International Association of Geodesy
NAVD88 : North America Vertical Datum of 1988
NGS : National Geodetic Survey
ODE : Ordinary Differential Equation
LSC : Least Squares Collocation
PoliMi : Politecnico di Milano
PDE : Partial Differential Equation
RMSE : Root Mean Square Error
RTM : Residual Terrain Model
SGM : Spectral Gravity-forward Modelling
STD : Standart Deviation
WLSC : Window Least Squares Collocation
XGM2016 : The Experimental Gravity Field Model 2016

SYMBOLS

Δ	: Laplace operator
V	: Gravitational potential
U	: Normal potential
W	: Actual potential
T	: Disturbing potential
r, θ, λ	: Spherical coordinates
φ, λ	: Latitude, longitude
g	: Gravity
γ	: Normal gravity
Δg	: Gravity anomaly
δg	: Gravity disturbance
P_{nm}	: Associated Legendre polynomials
Y_{nm}	: Surface spherical harmonics
C_{nm}, S_{nm}	: Spherical harmonic coefficients
ψ	: Spherical distance
G	: Gravitational constant
M	: Total mass of the Earth
R	: Mean radius of the Earth
ρ	: Crustal density
$S(\psi)$	: Stokes' function
$E\{x\}$	: Expectation of x
$M\{x\}$	: Average operator
l	: Observation vector
$\hat{s}$	: Estimated signal
$\Delta\psi$	: Interval length
C	: Covariance function
$C_{\Delta g \Delta g}$	: Auto-covariance of the gravity anomaly
$C_{\zeta \Delta g}$	: Cross-covariance between gravity and height anomaly
L	: Linear operator
σ_n^2	: Degree-variance
σ_ε^2	: Error degree-variance
R_B	: Depth of the Bjerhammar sphere
Δg_{res}	: Residual gravity anomaly
ζ_{res}	: Residual height anomaly
ζ	: Height anomaly
N	: Geoid undulation
h	: Ellipsoidal height
H	: Orthometric height
H^*	: Normal height

LIST OF TABLES

Page

LIST OF FIGURES

Page

CONTRIBUTION OF AIRBORNE GRAVIMETRY TO REGIONAL GEOID DETERMINATION BY LEAST SQUARES COLLOCATION

SUMMARY

With the development of technology, the use of Global Navigation Satellite Systems (GNSS) has become a widely recognized and essential element for the determination of the 3D position and time. Along with the satellite-based positioning techniques, the geoid based vertical datum studies for higher accuracy on height component has gained importance as well. In order to establish high-accuracy, high-resolution geoid models while considering the cost of the research, gravity data is started to be observed from different platforms. In recent years, airborne gravimetry has begun to be used to obtain gravity data over the places where the topography is challenging and therefore the ground-based measurements are hard to conduct.

To determine an accurate geoid model, accurate, dense, and homogeneously distributed gravity data is required. These requirements can be achieved by combining airborne and terrestrial gravity data. However, the characteristic difference of these two data sets (e.g. resolution, data coverage, the altitude of the observations) can cause inconsistencies in challanged areas. For this reason, this dissertation is dedicated to the investigation of terrestrial and airborne gravity data combination, and the contribution of airborne gravimetry in geoid determination.

In this study, terrestrial and airborne gravity data with the preliminary analysis are used in geoid computations of Colorado. Three geoid models with terrestrial only, airborne only, and combined gravity data are separately calculated over the area 36° - 38° N and 251.5° - 257° E using Least Squares Collocation (LSC) technique. These computations are carried out by using a covariance model that fits empirical covariances of both residual surfaces and downward continued airborne gravity anomalies since it is seen that the empirical covariances of both data sets are close to each other.

The computed models are externally validated on 87 historical sparse GPS/Leveling benchmarks. As a result, 6.6 cm, 6.4 cm, and 6.3 cm accuracy in terms of standard deviation is achieved for terrestrial only, airborne only, and combined models respectively. It is found that airborne gravity data shows the expected contribution especially in areas where the terrestrial data set is poor. The numerical and statistical outcomes are presented and discussed.

HAVA GRAVİMETRESİNİN EN KÜÇÜK KARELER KOLLOKASYON YÖNTEMİ İLE BÖLGESEL GEOİT BELİRLENMESİNE KATKISI

ÖZET

Uzun yıllar boyunca, dünya yüzeyinde bulunan bir noktanın ortometrik yüksekliği nivelman yöntemiyle elde edilmiş olan noktalar arasındaki yükseklik farklarına dayanarak hesaplanmıştır. Nivelman yönteminin doğası ve pratik sınırlamaları, bu yöntemin zorlu, kullanımının kısıtlı ve maliyetli olmasına sebep olmuştur. Teknolojinin gelişmesiyle birlikte Küresel Uydu Navigasyon Sistemleri (GNSS) kullanımı daha yaygın bir hale gelerek, konum ve yüksekliklerin belirlenmesinde önemli bir araç olmuştur. Ancak, bu uydu sistemleri ile elde edilen yüksekliklerin referans yüzeyi elipsoit olmasından dolayı pratik uygulamalarda ihtiyaç duyulan ortometrik yükseklik bilgisinin sağlanmasında yetersiz kalır. Bu sisteme dayanarak yüksek doğruluklu, verimli ve düşük maliyetli bir yükseklik sisteminin kurulabilmesi için yüksek doğruluklu bir gravimetrik geoit modeline ihtiyaç duyulur. Bu gravimetrik geoit model sayesinde elde edilmiş yüksekliklerin GNSS yöntemi kullanılarak elde edilmiş olan elipsoit yüksekliklerinden çıkarılması ile pratik uygulamalarda ihtiyaç duyulan ortometrik yükseklik bilgisi elde edilebilmektedir.

Geoidin tanımı yapılacak olur ise, fiziksel anlamda ortalama deniz yüzeyine yakınsayan ve karaların altından devam ettiği varsayılan özel bir eş potansiyel yüzeyi olarak yapılabilir. Bir eş potansiyel yüzey olan geoidin belirlenmesi, yeryüzünde konumu bilinen noktaların geoit yüksekliği bilgisinin sayısal olarak elde edilmesidir. Bu modellemenin yapılabilmesi için jeodezik sınır değer probleminin geoit yüzeyine indirgenmiş ölçülerin Stokes integrali veya benzer formüller yardımıyla çözülmesi gerekir.

Bununla birlikte, teoride geoit yüksekliklerine benzer bir başka yükseklik tanımı daha yapılmaktadır. Ancak bu yükseklikler, geoit yüksekliklerine kıyasla, referans yüzeyi ortalama deniz seviyesini değil, topoğrafyayı takip eder. Bu yüksekliklerin referans yüzeyine quasi-geoit denir. Topoğrafya ile bu referans yüzeyi olan quasi-geoit arasındaki mesafeye ise yükseklik anomalisi denir. Geoit yükseklikleri ile elipsoit yüksekliklerinin arasında kurulan ilişki gibi benzer bir ilişki yükseklik anomalileri ile elipsoit yükseklikleri arasında da kurulabilir. Bu noktadan ve Bouger gravite anomalilerine dayanarak geoit yükseklikleri ile yükseklik anomalileri arasında bir ilişkinin de kurulması mümkündür. Bu yükseklik anomalilerinin hesaplanmasında, geoit için geçerli olan yöntemlere bazı modifikasyonların yapılması yeterli olmaktadır.

Yeryüzündeki her noktada tam ve sürekliliği sağlayan gravite ölçüsünün varsayımı gerçekçi ve mümkün değildir. Bu durum, pratikte lokal alan için verilen noktalarda çözüm yapılarak sağlanır. Geoit modelleme sırasında jeofiziksel yapıyı daha iyi belirtebilmek için veri sıklığı ve dağılımı büyük önem taşır.

Gelişen teknoloji ile birlikte, gravite ölçmelerini kolaylaştıran farklı yöntemler ortaya çıkmaya başlamıştır. Özellikle son yıllarda kullanımı artan hava gravimetresi (airborne

gravimetry), değişken topografya yapısına sahip, yersel ölçüm yapılamayan yerlerde veri elde etmek için kullanılmaya başlanmıştır. Bu anlamda bölgesel geoit hesaplarına oldukça büyük katkılarda bulunarak, doğruluğun arttığı görülmüştür. Uçaktan gravite ölçülerinin topoğrafyaya indirilip, yersel veri ile birleştirilmesi, yüksek doğruluklu gravimetrik geoit hesabı için ihtiyaç duyulan verinin oluşturulması anlamında büyük önem taşır. Bununla birlikte, yersel ve hava gravite verilerinin çözünürlük, bu verilerin kapladıkları alan ve gravite ölçmelerinin yapıldığı yükseklikler gibi birçok yapısal farkları uyuşumsuzluklara neden olabilir. Bu nedenle, bu iki veri setinin uygun bir şekilde birleştirilmesi geoit belirleme için önemli bir basamaktır.

Bu tez kapsamında, yukarıda belirtilenlere dayanarak yersel ve hava gravite veri kombinasyonunun yapılması ve hava gravimetrisinin geoit belirlemede olan katkısı incelenmiştir. Bu çalışmada, halihazırda bulunan artık yersel ve topoğrafyaya indirgenmiş airborne gravite anomalileri kullanılarak Colorado/ABD bölgesinde En Küçük Kareler Kollokasyonu yaklaşımı ile geoit modellemesi yapılmıştır. Bu artık gravite anomaliler, global jeopotansiyel modelden elde edilen uzun ve topografik veriden elde edilen kısa dalga boyu katkılarının çıkarılması ile elde edilmiştir.

Sadece yersel, sadece hava gravimetresi ve bu verilerin kombinasyonundan oluşan bir veri seti kulanılarak üç adet quasi-geoit modeli hesaplanmıştır. Hesaplamalar En Küçük Kareler Kolokasyonu (EKK) yöntemi ile gerçekleştirilmiştir. Hesaplamalarda EKK metodunun kullanmasının sebebi, bu yöntemin bozucu potansiyele bağlı herhangi bir fonksiyonun tahmininde farklı veri tipleri, bir diğer anlamda farklı karakteristik özelliklere sahip olan veriler ve seyrek noktalardan oluşan veri setleri ile çalışabilmesidir. Bunun yanı sıra, ampirik değerlere dayanarak çözüm için veriye uygun bir model sunuyor olması da bu yöntemin kullanılmasındaki önemli noktalardan biridir.

Hesaplamalar için elde edilmiş kovaryans modeli, hem yersel hem topoğrafyaya indirgenmiş airborne artık gravite anomalilerinin ampirik kovaryans değerlerine uyum sağlamasından dolayı, veri kombinasyonu ve quasi-geoit hesaplamalarının hepsinde bu kovaryans modeli kullanılmıştır.

Öncelikli olarak sadece yersel ve sadece hava gravimetresine dayanan modeller 36° - 38° N ve 251.5° - 257° E sınırları içerisinde kalan $2' \times 2'$ grid üzerinde hesaplanmıştır. Sadece hava gravite verilerine ve sadece yersel verilere dayanarak hesaplanan yükseklik anomalilerinden sonra temizlenmiş yersel gravite anomalileri, topoğrafya yüzeyinde bulunan artık airborne gravite anomalileri ile yine EKK yöntemi kullanılarak, 36° - 38° N ve 251.5° - 257° E sınırları içerisinde kalan $2' \times 2'$ grid üzerinde birleştirilmiştir. Fakat bu birleştirilmiş veriye dayanan modelin hesabında, olası kenar etkilerinden kaçınmak için veri birleşiminde kullanılan alan sınırları, 36.2° - 37.8° N ve 251.8° - 256.8° şeklinde değiştirilmiştir.

Elde edilen modeller, bölgedeki bağımsız bir veri seti olan arşivsel GPS/Nivelman nokta ağı içindeki 87 nokta kullanılarak test edilmiştir. Bunun için hesaplanmış yükseklik anomalileri, bu noktalarda geoit yüksekliklerine dönüştürülmüştür. Sonuç olarak belirtilen 87 nokta üzerinde, sadece yersel, sadece hava gravimetresi ve birleştirilmiş veri ile hesaplanan modellerden sırası ile 6.6 cm, 6.4 cm ve 6.3 cm doğruluk elde edilmiştir. Elde edilen istatistiklerde de görüldüğü üzere en iyi sonuç birleştirilmiş veri setinden hesaplanan modelden alınmıştır. Bu durum, hava gravimetresinin kendisinden beklenen katkıyı sağladığını göstermektedir. Özellikle

dağlık bölgelerde bu katkı gözlenmektedir. Bunun sebebi ise, hızlı değişen topoğrafyanın yersel gravite ölçmelerini kısıtlamasıdır.

Fakat arşivsel GPS/Nivelman noktaları 5-6 cm'nin altındaki sonuçları test etmek için yeterli doğruluğa sahip değildir. Bu doğruluk probleminden dolayı daha net bir yourm ve kıyaslama sunulamadığı için, elde edilen modeller bu bölgede test amaçlı ölçülmüş yeni veri seti ile test edilmelidir.

1. INTRODUCTION

1.1 Statement of the Problem

The gravity field of the Earth, which reflects the inhomogeneous features of the Earth's interior and its surface, has been one of the topics that draws attention due to its contribution to many subjects in geoscience. Determination of the physical shape of the Earth, internal mass distribution, observing time variable effects, climatology, understanding lithosphere and interior of the Earth are just a few of the reasons why understanding the Earth's gravity field and the potential theory is important. For that matter, geodesy is the branch that is responsible for understanding and measuring the gravity field of the Earth. By the recent developments in technology, measuring the Earth's gravity field in a global and local scale is also improved. The major impact of this improvement can be seen especially in the developments in satellite gravity missions. That become a way to reach the needed accuracy for the gravity field determination. In this manner, three different successful satellite gravity missions like Challenging Minisatellite Payload (CHAMP) in 2000 (Reigber et al., 1999), Gravity Recovery and Climate Experiment (GRACE) in 2002 (Ward, 2004) and Gravity Field and Steady State Ocean Circulation Explorer (GOCE) in 2003 (Rebhan et al., 2000) came out. These extended the scientific work in determination of physical shape of the Earth, i.e. geoid, modeling of geostrophic currents and many like these.

In the local and regional scale, in the early years of 1990's the availability of Global Navigation Satellite Systems (GNSS) brought different techniques such as airborne and shipborne gravimetry to obtain accurate data at a higher resolution compare to both satellite and terrestrial gravity measurements. Especially, airborne gravimetry became an efficient way to collect and provide complementary data to both satellite and terrestrial observations. Combining gravity data sets which are obtained from different platforms, brings numerous advantages such as dense and homogeneously distributed observations. However, merging gravity data from different platforms leads to complexities due to the different characteristics of the data, i.e. the gravimeter used, frequency of the signal, determination of the height. There are several completed and

ongoing studies on how to merge airborne gravity data with the other data types. To do that, the downward continuation problem has to be surpassed. In the literature, many different methods are proposed such as Least Squares Collocation (Tscherning et al., 1998), planar collocation (Forsberg et al., 2001, 2007; Hvidegaard and Forsberg, 2002; Hwang et al., 2007), spectral weighting (Kern et al., 2003; Sjöberg, 2011) and among others. Also, Kern and Schwarz (2002); Li and Huang (2019); Müller and Mayer-Gürr (2005); Tziavos et al. (2005); Wang et al. (2004) present studies that give extended investigation and comparison of different downward continuation methods.

1.2 Thesis Objectives

The main objective of this thesis is determination and the validation of airborne gravity only, terrestrial gravity only, and combined quasi-geoid models by using the Colorado airborne gravity data analyzed and reduced by the AUTh and PoliMi sub-working groups (Grigoriadis et al., 2020) included in the working group under the International Association of Geodesy (IAG) Joint Working Group 2.2.2 (JWG2.2.2 - "The 1 cm geoid experiment").

1.3 Thesis Outline

This thesis is structured in five chapters. In Chapter 1, the general introduction on importance and applications of the Earth's gravity field, airborne gravimetry and a short review of the literature in this context are given. Chapter 2 presents the general background for the geoid determination and the used methodology in the this study. In Chapter 3, the used terrestrial, airborne data, and GPS/Leveling data sets are described. Chapter 4 is dedicated to numerical results of the downward continuation and geoid/quasi-geoid computation. As final, Chapter 5 presents the conclusion of the obtained results, discussions and recommendations based on these results.

2. METHODOLOGY

2.1 Geodetic Boundary Value Problems

The geoid is an equipotential surface that is defined through a constant potential value (W_0) and is estimared as the solution of a Boundary Value Problem (BVP) (Heiskanen and Moritz, 1967). BVP is a problem expressed by an Ordinary Differential Equation (ODE) or a Partial Differential Equation (PDE) on a domain where values are assigned on the physical boundary (McOwen, 2004). The solution of a BVP is a function satisfying the ODE or PDE inside the domain and taking the values given by boundary conditions at the boundary. In Geodesy, three different kind of boundary conditions are usually considered on the boundary (e.g. the Earth surface):

- Dirichlet: The value of the function is specified on the bounding surface.
- Neumann: On the bounding surface, the derivative of the function along the normal to surface is given.
- Robin: Mixed boundary condition where a linear combination of the value and the normal derivative of the function are specified on the bounding surface

The internal geodetic BVP is described by Poisson's equation where the all attracting masses are in the interior of the closed boundary surface, which is the Earth's surface. This represents the gravitational potential (V) for unit mass. For exterior domain which is mass-free, the BVP is described by Laplace's equation (Heiskanen and Moritz, 1967). The representation of Laplace's in Cartesian coordinates is

$$\Delta V(x,y,z) = 0 \tag{2.1}$$

where Δ is the Laplace operator. The Laplace's in spherical coordinates is

$$\Delta V = \frac{\partial^2 V}{\partial r^2} + \frac{2}{r}\frac{\partial V}{\partial r} + \frac{1}{r^2}\frac{\partial^2 V}{\partial \theta^2} + \frac{\cot\theta}{r^2}\frac{\partial V}{\partial \theta} + \frac{1}{r^2\sin^2\theta}\frac{\partial^2 V}{\partial \lambda^2} = 0 \tag{2.2}$$

where r, θ and λ are the spherical coordinates. In terms of geodesy, the boundary functions are geopotential values for Dirichlet boundary conditions, gravity

disturbances for Neumann, and gravity anomalies for Robin (Hofmann-Wellenhof and Moritz, 2006). Geodetic Boundary Value Problem (GBVP) for the Laplace equation can be classified in terms of the unknowns that one has to determine given the specified boundary conditions. In the fixed GBVP, the surface (S) is considered to be known, and also the boundary function gravity (g) (Heck, 1997). Thus, the solution for potential (W) is given as

$$W = F(S, g) \tag{2.3}$$

If the surface is unknown, it brings us to the definition of the free GBVP which is represented as the following equation.

$$S = F(g, W) \tag{2.4}$$

This GBVP is divided into two different categories depending on the type and the number of unknowns. The vectorial-free GBVP states that three-dimensional (3D) coordinates and the potential of the surface are unknown. Since the astronomical coordinates are used as boundary data, the vectorial-free GBVP can be called as the astronomical variant of Molodensky problem (Heck, 1997). In the scalar-free GBVP, only the vertical component of the surface and the potential are unknown. The geodetic coordinates are used in the scalar-free GBVP. Thus, it is described as the geodetic variant of Molodensky problem. The GBVPs are solved in a linearized form. This introduces the normal potential (U) which is an analytical approximation to the actual potential (W), and the gradient of the normal potential is the normal gravity (γ). The physical approximation for the linearization of Molodensky problem is defined by a known surface that is close the the surface of Earth(S). This approximate surface is called as telluroid ($\sum$) (Moritz, 1980).

On the other hand, if we assume that geoid is the boundary, all data has to be reduced to the geoid. This reduction can be done in several ways, although the simplest approach is the free-air reduction. The reduction to the sea level can be done by making an approximation for the density of the masses above the boundary (Heiskanen and Moritz, 1967). All the masses outside the geoid either are removed or shifted inside the geoid (Hofmann-Wellenhof and Moritz, 2006). This results with some effects on surface functions and normal gravity. The most common gravity observation is the gravity anomaly i.e.

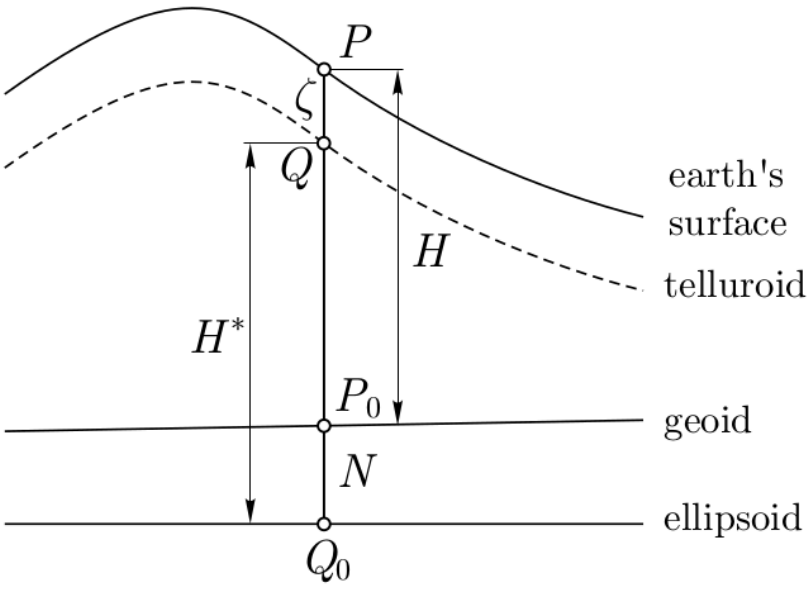

Figure 2.1 : Telluroid, change telluroid, Earth surface and ellipsoid (Wellenhof and Moritz, 2006)

$$\Delta g = g_P - \gamma_Q \tag{2.5}$$

Surface gravity anomalies (Δg) are obtained by Equation 2.5, where g_P represents the observed gravity at point P on the surface of the Earth, γ_Q is the normal gravity on telluroid that can be computed by using the normal gravity on ellipsoid as

$$\gamma_Q = \gamma_{Q_0}\left[1 - 2\left(1 + f + m - 2f\sin^2\varphi\right)\frac{H^*}{a} + 3\left(\frac{H^*}{a}\right)^2\right] \tag{2.6}$$

where γ_{Q_0} is the normal gravity on ellipsoid, f is the geometrical flattening of the ellipsoid, m is the ratio of centrifugal and gravity acceleration at its equator, a is the radius at the equator, and H^* is the normal height that is

$$H^* = h - \zeta \tag{2.7}$$

where h is the ellipsoidal height, and ζ is defined as the height anomaly which is the height from Earth's surface to telluroid. After surface gravity anomalies are computed, one can solve the GBVP to determine the geoid or quasi-geoid.

2.2 General Background for Geoid Determination

Depending on the modern theory, one can determine the gravimetric geoid by using surface gravity anomalies. Before that, one has to understand the relation of gravity disturbance and gravity anomaly to disturbing potential which will lead to the Stokes' equation.

2.2.1 Stokes' Equation

The gravity disturbance (δg) is the magnitude difference between the gravity at point P on the surface and the normal gravity (γ) at the same point P. The linear combination of gravity disturbance and gravity anomaly describes a boundary condition which is known as the golden formula of physical geodesy (see Equation 2.8).

$$\Delta g = \delta g - \frac{2}{r}T \tag{2.8}$$

In the Equation 2.8, r represents the radius of the Earth, T represents the disturbing potential (see Equation 2.9) which is a harmonic function.

$$T = W - U \tag{2.9}$$

δg can be expressed in another way as (Heiskanen and Moritz, 1967)

$$\delta g = -\left(\frac{\partial W}{\partial r} - \frac{\partial U}{\partial r}\right) = -\frac{\partial T}{\partial r} \tag{2.10}$$

To understand the given equation and the relation between Δg and δg, one needs to focus on the term $-\frac{\partial T}{\partial r}$. Thus, anomalous potential which is a harmonic function, can be expressed more elegantly. Since every function which is harmonic can be expanded into a series of surface spherical harmonics (see Equation 2.11), same procedure is applied to expand the disturbing potential in spherical harmonics

$$f(\vartheta,\lambda) = \sum_{n=0}^{\infty} Y_n(\vartheta,\lambda) = \sum_{n=0}^{\infty}\sum_{m=0}^{n} [a_{nm}P_{nm}(\cos\vartheta)\cos m\lambda + b_{nm}P_{nm}(\cos\vartheta)\sin m\lambda] \tag{2.11}$$

In Equation 2.11, $P_{n,m}$ is the associated Legendre functions of degree n order m, $a_{n,m}$ and $b_{n,m}$ are the coefficients determined according to the orthogonality relations which will bring the integral equation of the surface spherical harmonics

(Hofmann-Wellenhof and Moritz, 2006). Thus, one can write

$$T = T(r,\theta,\lambda) = \sum_{n=0}^{\infty} \left(\frac{R}{r}\right)^{n+1} T_n(\theta,\lambda) \tag{2.12}$$

T_n in Equation 2.12 is the Laplace's surface harmonics (see Equation 2.11) and R is the mean Earth radius. The derivative of T given in 2.12 with respect to r gives the gravity disturbance δg:

$$\delta g = -\frac{\partial T}{\partial r} = \frac{1}{r}\sum_{n=0}^{\infty}(n+1)\left(\frac{R}{r}\right)^{n+1} T_n(\vartheta,\lambda) \tag{2.13}$$

Inserting Equation 2.12 and 2.13 into Equation 2.8, the gravity anomaly can be calculated as:

$$\begin{aligned}\Delta g &= \frac{1}{r}\sum_{n=0}^{\infty}(n-1)\left(\frac{R}{r}\right)^{n+1} T_n(\vartheta,\lambda) \\ &= \sum_{n=0}^{\infty}\Delta g_n(\vartheta,\lambda)\end{aligned} \tag{2.14}$$

To obtain the gravity anomaly on geoid, r has to be taken as R which cancels the term $\left(\frac{R}{r}\right)^{n+1}$. In the given equation, the term $n = 0$, which represents the total mass, and $n = 1$, which represents the offset of the coordinate systems origin from centre of mass, vanishes due to the fact that $n = 1$ results as $\Delta g = 0$, and $n = 0$ gives $T_0/R = 0$ because total mass (GM) is same for both actual and normal potential (Moritz, 1980). Thus, n can start from 2. By comparing the given equivalences in Equation 2.14 and transforming the series expansion to the integral form, the following formula is obtained (see Equation 2.15) where ψ is the spherical distance between two points.

$$\begin{aligned}T &= \frac{R}{4\pi}\iint_{\sigma}\left[\sum_{n=2}^{\infty}\frac{2n+1}{n-1}P_n(\cos\psi)\right]\Delta g\, d\sigma \\ &= \frac{R}{4\pi}\iint_{\sigma} S(\psi)\Delta g\, d\sigma\end{aligned} \tag{2.15}$$

The term inside the brackets is the Stokes' function in terms of Legendre polynomials (for analytical expression, see Wellenhof and Moritz,2006, eq. 2-305). From the Brun's theorem, the geoid undulation is then expressed as

$$N = \frac{R}{4\pi\gamma_0}\iint_{\sigma}\Delta g S(\psi)\, d\sigma \tag{2.16}$$

However, according to Molodensky's theory this formula is expressed through the definition of height anomaly by using the surface gravity anomalies. The advantage of obtaining height anomalies is that it eliminates the error related to density assumption

which is used in mass reduction (Hofmann-Wellenhof and Moritz, 2006). By adding the correction terms containing the effect of topography (Molodensky's correction) and also the distance between the geoid and the quasi-geoid ($\frac{\bar{g}-\bar{\gamma}}{\bar{\gamma}}H$), it is possible to determine the geoid from surface gravity anomalies.

$$N = \frac{R}{4\pi\gamma_0}\iint_\sigma \left[\Delta g - \frac{\partial \Delta g}{\partial h}(h-h_P)\right] S(\psi)d\sigma + \frac{\bar{g}-\bar{\gamma}}{\bar{\gamma}}H \tag{2.17}$$

In Equation 2.17, the term expressed in the brackets means that the surface gravity anomalies are analytically downward continued from observation surface to level of computation point P that is on telluroid. Analytical continuation is described as extending the domain in which the boundary function is defined, by Taylor series (Hofmann-Wellenhof and Moritz, 2006). Since the functions that satisfy Laplace's equation are harmonic, analytical continuation can be called as harmonic continuation. To describe it better in terms of physical geodesy, the continuation of exterior potential is possible in case of a regular harmonic function. However, the mass structure and the density change outside the reference ellipsoid create irregularity which results with the problems in analytical continuation down to the level of computation point (Hofmann-Wellenhof and Moritz, 2006). Despite of this problem, it is possible to analytically continue the function by Runge-Krarup theorem.

2.2.2 Runge-Krarup Theorem

As it is stated before a regular harmonic continuation is possible by Runge's theorem. Assume that there is a compact set (K) which is closed and bounded, and also there are two open sets (Γ, Ω) in $\mathbb{R}^3$ (Moritz, 1980). Their boundaries posses a similar form as a sphere and each of the sets is a subset of the other ($K \subset \Gamma \subset \Omega$). Let there be a harmonic and regular function (f) in the open set Γ, and assume a limit (ε) that is arbitrarily small. According to the given assumptions, Runge's theorem states that there has to be a function (g) that is harmonic in Ω (see Figure 2.2) so that

$$| f - g | < \varepsilon \tag{2.18}$$

The relation of Runge's theorem to physical geodesy is called as Runge-Krarup theorem. In terms of physical geodesy, if there is a harmonic function that is regular outside the boundary, in our case the surface of the Earth, it can be approximated by functions harmonic outside a defined sphere inside the Earth which is called as

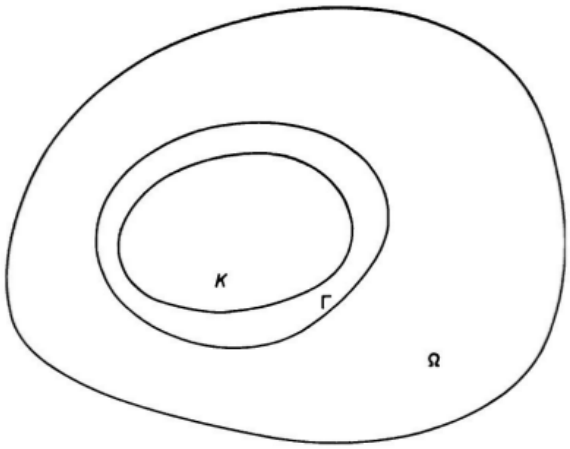

Figure 2.2 : Compact (K) and open sets (Γ, Ω) (Moritz, 1980)

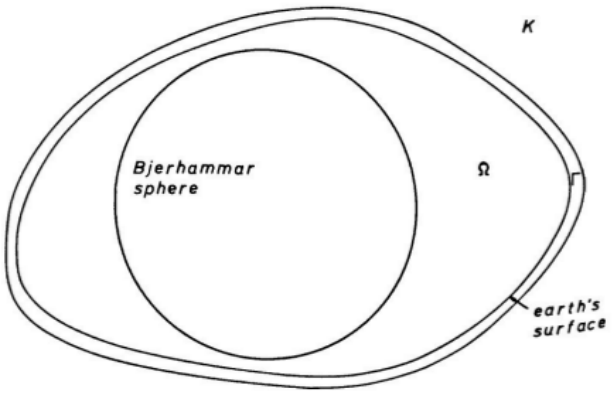

Figure 2.3 : The relation of the sets in physical geodesy (Moritz, 1980)

Bjerhammar sphere (see Figure 2.3) (Moritz, 1980). The functions f, g in Equation 2.18 become the disturbing potentials for different domains. If a function can be analytically continued down to the computation point, then finding the potential from discrete data is possible.

2.2.3 Theory of Least Squares Collocation (LSC)

Least Squares Collocation can be described as an optimization problem that minimizes the mean square error depending on a group of estimators which remain unchanged under certain classes of transformations (Moritz, 1980). In terms of geodesy, the function to be predicted is the disturbing potential which is obtained depending on the Runge-Krarup theorem by saying that T is harmonic down to the Bjerhammar sphere. To understand the theory of LSC, one needs to understand the basics of least squares prediction and the covariance function on which the LSC estimation is based.

2.2.3.1 Basics of least squares prediction

LSC is based on the concept of stochastic process. Stochastic process can be described as a family of random variables from probability space into a state space. In a stochastic process, covariances can be computed according to the formula

$$\mathrm{Cov}\left\{f(x_1), f(x_2)\right\} = E\left\{\left[f(x_1) - E\left\{f(x_1)\right\}\right]\left[f(x_2) - E\left\{f(x_2)\right\}\right]\right\} \tag{2.19}$$

Covariances of variables that belong to the same function define the auto-covariances. If this is computed for different functions, it gives the cross-covariances. Accordingly, one can set the relation between the observation vector (l) and the estimated signal ($\hat{s}$) through the covariance matrices. The difference between $\hat{s}$ and s gives the error vector which will lead to the construction of error covariance matrix ($E\{\varepsilon\varepsilon^T\}$). The best scenario can be defined as the unbiased linear estimation which means that the expectation of estimation equals to zero. Thus, the matrix in the linear estimation (H) has to be determined by the following formula

$$\varepsilon\varepsilon^T = (Hl - s)(Hl - s)^T = Hll^T H^T - Hls^T - sl^T H^T + ss^T \tag{2.20}$$

The expectation of this expression gives the description of error covariance matrix ($C_{\varepsilon\varepsilon}$). Since it is known that $E\{ll^T\}$, $E\{ss^T\}$, $E\{ls^T\}$ and $E\{sl^T\}$ represent the auto and cross covariances, the equation becomes

$$\begin{aligned} C_{\varepsilon\varepsilon} &= HC_{ll}H^T - C_{sl}H^T - HC_{ls} + C_{ss} \\ &= C_{ss} - C_{sl}C_{ll}^{-1}C_{ls} + (H - C_{sl}C_{ll}^{-1})C_{ll}(H - C_{ls}C_{ll)}^{-1})^T \end{aligned} \tag{2.21}$$

The given equation has parts which are both dependent and independent from H matrix. If H is taken as $C_{sl}C_{ll}^{-1}$, the part that includes the term H is eliminated from the equation which becomes

$$C_{\varepsilon\varepsilon} = C_{ss} - C_{sl}C_{ll}^{-1}C_{ls} \tag{2.22}$$

this leads to the description of the best linear estimate of the signal in terms of the observation vector l, i.e.

$$\hat{s} = C_{sl}C_{ll}^{-1}l \tag{2.23}$$

The given equation is the representation of least squares prediction. In terms of physical geodesy, the observation matrix l can include the gravity anomalies, height anomalies or other gravity related functional. As an example, let l be a vector of

gravity anomalies without any errors and that s is the vector of gravity anomalies at a given prediction point. In this case, the estimation equation (Equation 2.23) becomes

$$\Delta g_p = \begin{bmatrix} c_{p1} & c_{p2} & \cdots & c_{pq} \end{bmatrix} \begin{bmatrix} c_{11} & c_{12} & \cdots & c_{1q} \\ c_{21} & c_{22} & \cdots & c_{2q} \\ \vdots & \vdots & & \vdots \\ c_{q1} & c_{q2} & \cdots & c_{qq} \end{bmatrix}^{-1} \begin{bmatrix} \Delta g_1 \\ \Delta g_2 \\ \vdots \\ \Delta g_q \end{bmatrix} \tag{2.24}$$

where C_{ij} are computed based on the auto covariance of gravity anomalies.

2.2.3.2 The covariance function

As mentioned in the previous section, in collocation, the solution relies on the covariance function of the geodetic observations that will be constructed from a basic function $K(P,Q)$ i.e., the covariance function of the anomalous potential $T(P)$. (Moritz, 1980). This basic function, $K(P,Q)$, describes a relation between the disturbing potential at point P and Q by averaging the product of $T(P)$ and $T(Q)$, that is

$$K(P,Q) = K(\psi) = M\{T(P)T(Q)\} \tag{2.25}$$

This average operator applies over the whole sphere which describes the homogeneity through this identity. Depending on this, the function $K(P,Q)$ can be expressed by the spherical distance between point P and Q as in equation above where spherical distance (ψ) is defined as (Moritz, 1980).

$$\cos\psi = cos\theta\cos\theta^{'} + \sin\theta\sin\theta^{'}cos(\lambda - \lambda^{'}) \tag{2.26}$$

One can represent the Equation 2.25 as

$$K(\psi) = \sum_{n=2}^{\infty} k_n P_n(\cos\psi) \tag{2.27}$$

where P_n is the Legendre polynomial. In the given formula, the degree terms $n = 0, 1$ are excluded to obtain a centered expectation by the fact that all the coefficients ($n > 0$) vanish to zero (Moritz, 1980). Since T is a function that is harmonic outside the boundary, the expression stated in Equation 2.27 can turn into a form as in Equation 2.28 which is the formula of the covariance function of disturbing potential.

$$K(P,Q) = K(\psi) = \sum_{n=2}^{\infty} k_n \left(\frac{R^2}{r_P r_Q}\right)^{n+1} P_n(\cos\psi_{PQ}) \tag{2.28}$$

k_n is the degree-variances of the disturbing potential, defined as

$$k_n = \sum_{m=-n}^{n} T_{nm}^2 \tag{2.29}$$

However, this expression requires the knowledge of disturbing potential. Since usually the gravity anomalies are the given data, both auto ($C_{\Delta g \Delta g}$) and cross covariances ($C_{T\Delta g}$) are needed in order to determine the quasi-geoid without the direct knowledge of T. From Equation 2.14, the relationship between disturbing potential and gravity anomalies is known. By introducing the linear operator (L), once can write $\Delta g = L_g\{T\}$ (see Equation 2.8 and 2.10). Since one can also assume that

$$L_g\{f\} = \sum_{n=2}^{\infty} L_g^n f_n \tag{2.30}$$

where L_g^n is

$$L_g^n = \frac{n-1}{R}\left(\frac{R}{r}\right)^{n+1} \tag{2.31}$$

based on Equation 2.25 and 2.31, one can obtain the following expressions

$$\begin{aligned} M\{\Delta g_P \Delta g_Q\} &= \sum_{n=2}^{\infty} L_{g,P}^n L_{g,Q}^n M\{T_n T_n\} \\ &= \sum_{n=2}^{\infty} \frac{(n-1)^2}{R^2}\left(\frac{R^2}{r_P r_Q}\right)^{n+1} k_n P_n(\cos\psi_{PQ}) \end{aligned} \tag{2.32}$$

By saying that degree-variances of gravity anomalies are equal to $c_n = \left(\frac{n-1}{R}\right)^2 k_n$, one can obtain the following equation

$$C(\psi, r_P, r_Q) = \sum_{n=2}^{\infty}\left(\frac{R^2}{r_P r_Q}\right)^{n+1} c_n P_n(\cos\psi_{PQ}) \tag{2.33}$$

which is the covariance function of the gravity anomaly. This holds for global applications. In local applications, a better covariance function can be obtained with more different models (Tscherning and Rapp, 1974).

In order to estimate parameters in the model covariances one should assume that the stochastic process is stationary and ergodic. Stationarity refers to the distribution of the random variables. More specifically, in a stationary stochastic process all random variables have the same distribution function and the statistical properties do not change in space. On the other hand, ergodicity allows estimating the covariance based on the mean over the sphere. Thus, the estimation of covariances for given spherical

distance can be evaluated by summation of products of a set of observed values inside an interval (see Equation 2.34)

$$\psi - \frac{\Delta\psi}{2} < \psi_i < \psi + \frac{\Delta\psi}{2} \tag{2.34}$$

where $\Delta\psi$ is the interval length. Hence, this gives the following equation that represents the empirical covariances.

$$C(\psi) = \frac{1}{N_j} \sum_{k,i}^{N_j} f(\varphi_k, \lambda_k) \cdot g(\varphi_i, \lambda_i) \tag{2.35}$$

When using local data, the empirical covariance should be fitted with local covariance models. This can be done by the degree-variances which now should be taken into account by the fact that in practice residual gravity anomalies are used. This leads to the definition of error degree-variances (σ_ε), and to local covariance models of the form

$$\begin{aligned} C_{TT}(r_P, r_Q) = &\sum_{n=N_{max}+1}^{+\infty} \sigma_n^2 \left(\frac{R_B^2}{r_P r_Q}\right)^{n+1} P_n(\cos\psi_{PQ}) \\ &+ \alpha \sum_{n=2}^{N_{max}} \sigma_\varepsilon^2 \left(\frac{R^2}{r_P r_Q}\right)^{n+1} P_n(\cos\psi_{PQ}) \end{aligned} \tag{2.36}$$

This equation is the model of the local covariance function ($C_{TT}(r_P, r_Q)$) where R_B is the depth of the Bjerhammar sphere, σ_n is the anomaly degree variances, α is the calibration constant, σ_ε is the error degree-variances, and N_{max} is the degree of the geopotential model used in reducing the data. By propagation of covariance the covariance function can be expressed for the other functionals. As an example, the covariance function between gravity anomaly and disturbing potential is

$$\begin{aligned} C_{\Delta g T}(P, Q) = &\frac{1}{r_p} \sum_{n=N_{max}+1}^{+\infty} \sigma_n^2 (n-1) \left(\frac{R_B^2}{r_P r_Q}\right)^{n+1} P_n(\cos\psi_{PQ}) \\ &+ \alpha \sum_{n=2}^{N_{\max}} \sigma_\varepsilon^2 \left(\frac{R^2}{r_P r_Q}\right)^{n+1} P_n(\cos\psi_{PQ}) \end{aligned} \tag{2.37}$$

where the first part of the expression in Equation 2.36 is multiplied by the term $\frac{(n-1)}{r_P}$. Similarly, the auto-covariance of the gravity anomaly and the cross-covariance between gravity and height anomaly are

$$\begin{aligned} C_{\Delta g \Delta g}(P, Q) = &\frac{1}{r_P r_Q} \sum_{n=N_{max}+1}^{+\infty} \sigma_n^2 (n-1)^2 \left(\frac{R_B^2}{r_P r_Q}\right)^{n+1} P_n(\cos\psi_{PQ}) \\ &+ \alpha \sum_{n=2}^{N_{\max}} \sigma_\varepsilon^2 \left(\frac{R^2}{r_P r_Q}\right)^{n+1} P_n(\cos\psi_{PQ}) \end{aligned} \tag{2.38}$$

$$C_{\zeta\Delta g}(P,Q) = \frac{1}{r_p \gamma_Q} \sum_{n=N_{max}+1}^{+\infty} \sigma_n^2(n-1) \left(\frac{R_B^2}{r_p r_Q}\right)^{n+1} P_n(\cos\psi_{PQ}) + \alpha \sum_{n=2}^{N_{\max}} \sigma_\varepsilon^2 \left(\frac{R^2}{r_P r_Q}\right)^{n+1} P_n(\cos\psi_{PQ}) \tag{2.39}$$

2.2.4 The Remove-Restore Technique

In local gravity field determination, some modifications are necessary due to the fact that data are given only in a limited part of the Earth. The limitation of the area results in lack of signal representation. Thus, in regional and local geoid determination, one should follow the Remove - Restore principle which is based on the assumption that gravity field signal can be divided into three components as long, medium and short wavelength.

$$\Delta g = \Delta g_1 + \Delta g_2 + \Delta g_3 \tag{2.40}$$

The low frequency part of the signal includes the trends and systematic effects of the global gravity field (Δg_1) (see Equation 2.48), where the high frequency part (Δg_2) includes the information coming from topography (see Equation 2.42), and the remaining part is coming from the residual field (Δg_3) (Hofmann-Wellenhof and Moritz, 2006). In this sense, the low frequency part of the signal is approximated by Global Geopotential Models (GGMs) which represent functionals of the gravity field at global scale. Therefore, in Remove - Restore procedure, a suitable GGM is chosen to remove the effect of the gravity field outside the study area by subtracting it from the observed data. In term of gravity anomaly, this can be computed as

$$\Delta g_{ggm}(\varphi,\lambda,r) = \frac{GM}{r^2} \sum_{m=0}^{L_{max}} \left[\cos(m\lambda) \sum_{n=L_{min}}^{L_{max}} (n-1) \left(\frac{R}{r}\right)^n C_{nm} P_{nm} \sin(\varphi) + \sin(m\lambda) \sum_{n=L_{min}}^{L_{max}} (n-1) \left(\frac{R}{r}\right)^n S_{nm} P_{nm} \sin(\varphi) \right] \tag{2.41}$$

where L_{max} is the maximum degree/order of GGM, C_{nm} and S_{nm} are the GGM coefficients. Subtracting the low frequency part gives a reduced gravity field where the effect of the attraction that comes from Earth's interior and upper mantle is removed. However, the contribution of GGM is limited due to the fact that it contains information about Earth's gravity field up to a maximum degree. After removal, the signal still contains the medium and the high frequency components, which are the signal contribution of topography (Forsberg and Tscherning, 1997). This high

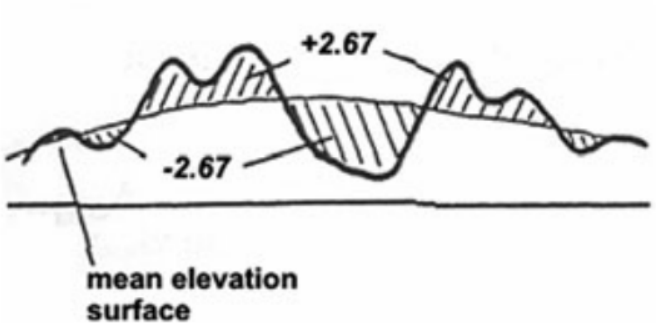

Figure 2.4 : The geometry of RTM reduction. Topography above the mean elevation surface is removed and the valleys are filled(Forsberg, 1984).

frequency contribution can be computed by using the Residual Terrain Model (RTM). A smooth mean elevation surface and a detailed Digital Terrain Model (DTM) are used to compute the topographic effect on gravity of the RTM reduction where the crustal density is fixed as 2.67 g/cm^3. The mean elevation surface can be computed either by using a global topography model up to the degree and order of the removed GGM or by filtering the local terrain heights (Forsberg, 1984).

Yet, the removal of the masses below the reference surface causes inconsistencies due to the non-harmonicity (Hirt et al., 2019). To overcome this problem, either harmonic correction or spectral techniques should be applied.

In this thesis, topographic models which are developed by spectral solution, are used to compute the RTM effect by combining those models. This spectral method is a linear combination of spherical harmonics which solves the non-harmonicity problem by dividing the gravity signal of the reference topography (Δg^{HREF}) into three components as

$$\begin{aligned} \Delta g^{\mathrm{HREF}} &= \Delta g^{\mathrm{SGM}}_{0\ldots\infty} \\ &= \Delta g^{\mathrm{SGM}}_{0..N} + \Delta g^{\mathrm{SGM}}_{N+1\ldots kN} + \Delta g^{\mathrm{SGM}}_{kN+1\ldots\infty} \\ &\approx \Delta g^{\mathrm{SGM}}_{0\ldots N} + \Delta g^{\mathrm{SGM}}_{N+1\ldots kN} \end{aligned} \tag{2.42}$$

where the first term ($\Delta g^{SGM}_{0\ldots N}$) is described as the bulk of the signal, and the second term is the ultra-high degree Spectral Gravity-forward Modelling (SGM) component ($\Delta g^{SGM}_{N_1\ldots N_2}$) (Hirt et al., 2019) as

$$\Delta g^{\mathrm{SGM}}_{N1\ldots N2} = \frac{GM}{r^2} \sum_{n=N1}^{N2} (n-1) \left(\frac{R}{r}\right)^n \sum_{m=-n}^{n} \bar{V}_{nm} \bar{Y}_{nm}(\varphi, \lambda) \tag{2.43}$$

where $\bar{Y}_{nm}$ are the fully normalized surface spherical harmonics, and $\bar{V}_{nm}$ are the topographic potential coefficients which are obtained (Hirt et al., 2019) based on

$$\bar{V}_{nm} = \frac{4\pi R^3 \rho}{(2n+1)M} \sum_{p=1}^{p_{\min}} \frac{\prod_{i=1}^{p}(n-i+4)}{p!(n+3)} H_{nm}^{(p)} \tag{2.44}$$

where ρ is the crustal density, M is the mass of the Earth, H_{nm} are fully normalized spherical harmonic height coefficients which are generated by a Digital Elevation Model (DEM). By using Equation 2.42, RTM effect of gravity anomaly signal (Hirt et al., 2019) is presented as

$$\Delta g_{rtm} = \Delta g^{\mathrm{H}} - \Delta g^{\mathrm{HREF}} \tag{2.45}$$

where Δg^{H} is the gravity anomaly signal of the topographic mass with orthometric height H at the observation point.

For instance, ERTM2160 (Earth Residual Terrain Modelled-gravity field) (Hirt et al., 2014) and Earth2014 (Hirt and Rexer, 2015) are the models developed by the method explained above. These models are provided in grid form for the users, and can be downloaded from (http://ddfe.curtin.edu.au/models/).

As it is mentioned in Section 3.3, since the GGM is expanded up to d/o 720, Earth2014 model from d/o 720 (Hirt and Rexer, 2015) up to d/o 2160 and ERTM2160 (Hirt et al., 2014) up to d/o 96000 are used to interpolate the RTM effect for the given d/o at the observation points. The interpolated values are summed to obtain RTM effect.

After the reduction of RTM effect, the residual gravity anomalies (Δg_{res}) is obtained as

$$\Delta g_{res} = \Delta g - \Delta g_{ggm} - \Delta g_{rtm} \tag{2.46}$$

The residuals used in this thesis are obtained from Grigoriadis et al. (2020) within the scope of the International Association of Geodesy (IAG) Joint Working Group 2.2.2 (JWG2.2.2 – "The 1 cm geoid experiment").

The obtained residual gravity anomalies can be used to estimate the residual height anomalies using e.g. LSC. To obtain the height anomalies, the residual height anomalies has to be restored as they removed by using the same models and parameters. In the restore step, the removed components are added for the height anomaly as

$$\zeta = \zeta_{res} + \zeta_{ggm} + \zeta_{rtm} \tag{2.47}$$

where ζ_{ggm} is computed as

$$\zeta_{ggm}(\varphi,\lambda,r) = \frac{GM}{\gamma r^2}\sum_{m=0}^{L_{max}}\left[\cos(m\lambda)\sum_{n=L_{min}}^{L_{max}}\left(\frac{R}{r}\right)^n C_{nm}P_{nm}\sin(\varphi) + \right.$$
$$\left. + \sin(m\lambda)\sum_{n=L_{min}}^{L_{max}}\left(\frac{R}{r}\right)^n S_{nm}P_{nm}\sin(\varphi)\right] \tag{2.48}$$

and ζ_{rtm} is obtained by interpolating RTM effect in terms of height anomaly using Earth2014 from d/o 720 up to d/o 2160 and ERTM2160 up to d/o 96000. In these presented models, the RTM effect in terms of height anomaly is developed as

$$\zeta_{rtm} = \zeta^{\mathrm{H}} - \zeta^{\mathrm{HREF}} \tag{2.49}$$

where ζ^{HREF} is

$$\zeta^{\mathrm{HREF}} \approx \zeta^{\mathrm{SGM}}_{0\ldots N} + \zeta^{\mathrm{SGM}}_{N+1\ldots kN} \tag{2.50}$$

and $\zeta^{\mathrm{SGM}}_{N1\ldots N2}$ is given as

$$\zeta^{\mathrm{SGM}}_{N1\ldots N2} = \frac{GM}{\gamma r^2}\sum_{n=N1}^{N2}\left(\frac{R}{r}\right)^n \sum_{m=-n}^{n}\bar{V}_{nm}\bar{Y}_{nm}(\varphi,\lambda) \tag{2.51}$$

2.2.5 Airborne Gravimetry in Geoid Computation

The use of airborne data in gravity field determination requires downward continuation of the gravity data from flight altitude either to the terrain or the geoid/quasi-geoid (Forsberg and Olesen, 2010). By downward continuation, it is possible to form a third combined gravity data set with ground data which can be dense and homogeneously distributed. Various different techniques can be performed to downward continue the airborne data such as radial basis function, Fast Fourier Transformation (FFT), Poisson's equation, Least Squares Collocation (LSC) and so on. Many of these methods, specifically integral based methods, require a stable flight altitude in order to have a stable downward continuation process; however, this is not always possible (Forsberg and Olesen, 2010). Especially, the surveys that is held in a wide area with changing topography leads to change flight altitudes. For observations with unstable flight altitudes, it might be better to perform downward continuation with a method that can consider the heights. Therefore, least squares collocation can be chosen as the method for downward continuation due to the fact that the point heights are taken into account in LSC. Additionally, stabilization of downward continuation can be done by using the Remove - Restore technique.

In LSC, the estimation of the downward continued residual gravity anomalies ($\hat{s}$) can be computed based on the Equation 2.23 and 2.38. It should be reminded that Equation 2.23 does not consider the noise within the observation. However, observations contain noise. Thus, Equation 2.23 becomes

$$\hat{s} = C_{sx}\left[C_{ss} + D\right]^{-1}\left(\Delta g + n_{\Delta g}\right) \tag{2.52}$$

where C_{sx} and $C_s s$ are the model covariances that represents the relation between the gravity anomaly on ground (s) and at the flight altitude (x), and D is the diagonal noise matrix.

After the downward continuation of the residual gravity anomalies to terrain, airborne data can be used either directly for the estimation of the height anomalies or merged with residual surface gravity anomalies. However, before any further computation, the empirical covariance of downward continued residuals should be computed and checked to see if the model covariance of ground data fits the empirical covariance of downward continued residuals. If the model covariance and the empirical covariances are in a good agreement, same parameters that are used in downward continuation (depth of the Bjerhammar sphere, variance of the data, the degree of the error degree variances, noise variance) can be used for combining the data sets and quasi-geoid computation.

If the aim is forming a combined data set, it might be better to clean the terrestrial data before combining the data sets. Downward continued airborne gravity anomalies and the cleaned surface gravity anomalies can be combined as in Equation 2.52 to obtain a combined grid which can be used in the estimation of residual height anomalies.

Since the residual gravity anomalies are known for downward continued airborne, surface and combined data, the residual height anomalies ($\hat{\zeta}_{res}$) can be estimated as

$$\hat{\zeta}_{res} = C_{\zeta\Delta g}\left(C_{\Delta g\Delta g} + \sigma^2_{n_{\Delta g}} I\right)^{-1}\left(\Delta g_{res} + n_{\Delta g}\right) \tag{2.53}$$

where $C_{\zeta\Delta g}$ is the cross covariance (see Equation 2.39), $C_{\Delta g\Delta g}$ is the auto covariance (see Equation 2.38), $\sigma^2_{n_{\Delta g}}$ is the noise variance, I is the unit matrix, and $\left(\Delta g_{res} + n_{\Delta g}\right)$ represents the observation and its noise. By restoring the low and high frequency contributions as in Equation 2.47, the quasi-geoid is obtained.

A detailed frame of the quasi-geoid computation by LSC is given in Figure 2.5 for terrestrial data. Additionally, in Figure 2.6 same flow is given for airborne data. It

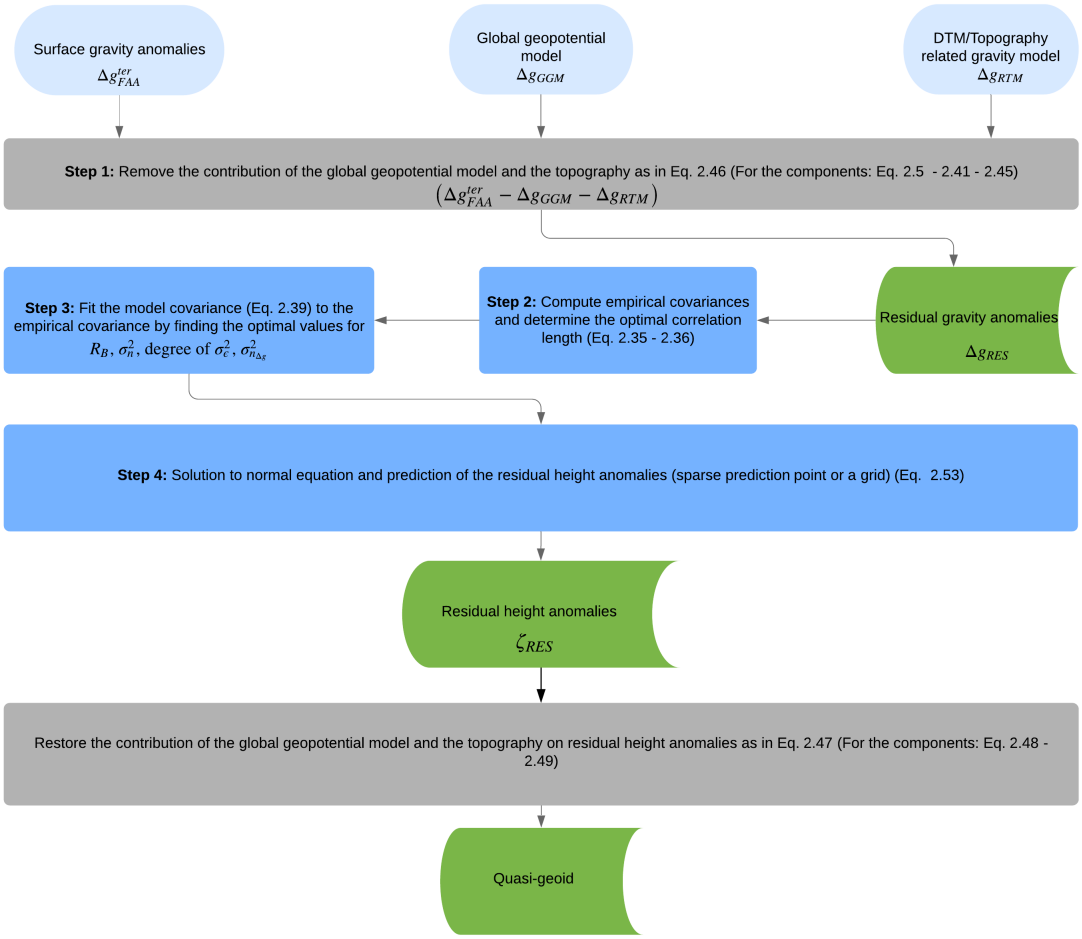

Figure 2.5 : Flowchart of the Least Squares Collocation process for terrestrial data

starts with downward continuation of airborne data to the Earth surface, which follows by merging the downward continued airborne gravity anomalies with surface gravity anomalies, and compute both airborne only and combined quasi-geoid models. For the downward continuation of the airborne data, only free-air gravity anomalies at flight level are used. This procedure is followed by computation of both airborne only and combined quasi-geoid model. A simplified version of these flowcharts is given in Figure C.1 with job files descriptions given in Appendix C and directory given in Table C.1.

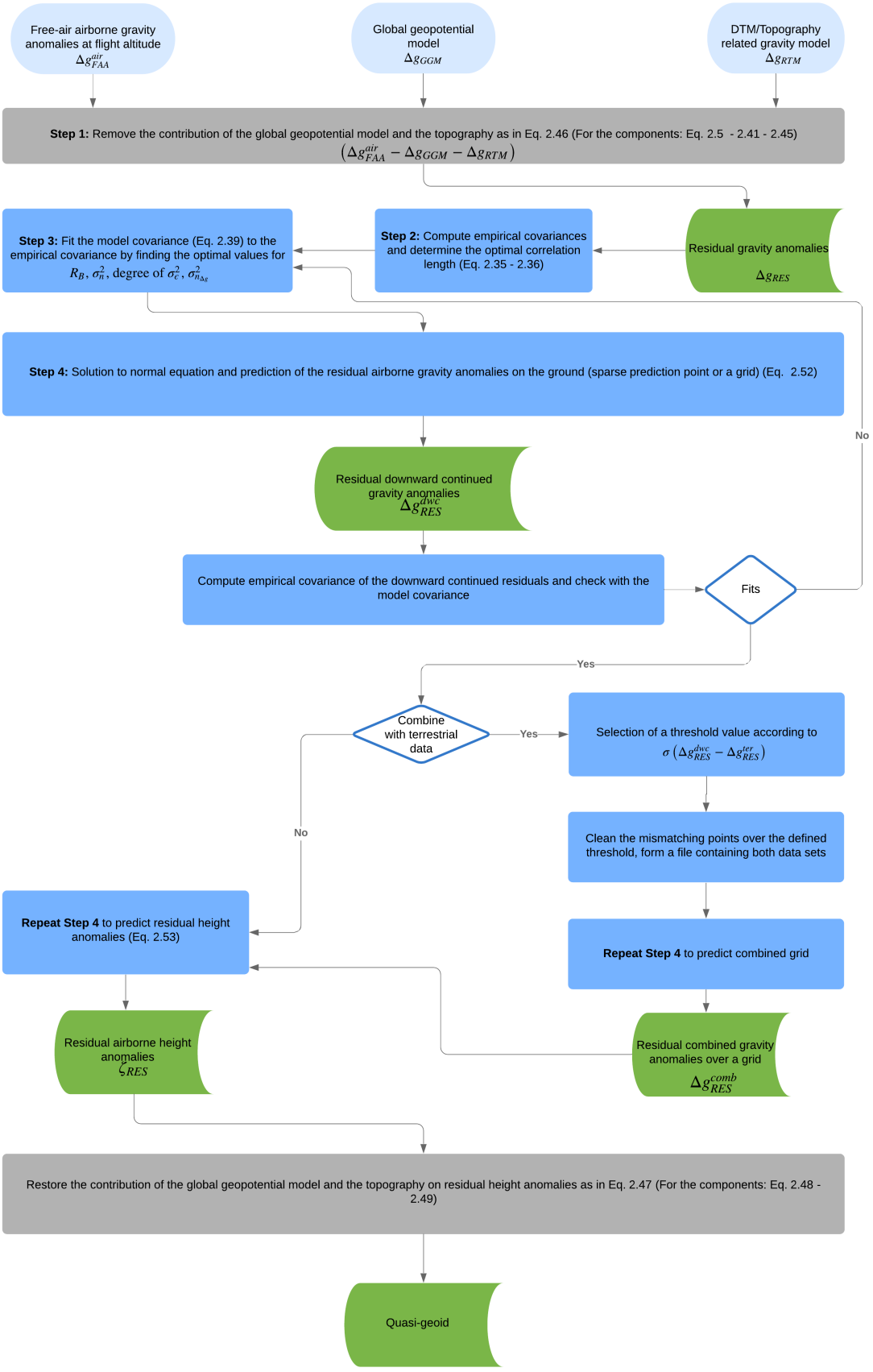

Figure 2.6 : Flowchart of the Least Squares Collocation process for airborne and combined data

3. DATA SETS AND STUDY AREA

In this chapter, the used data sets including terrestrial and airborne gravity measurements, and historical GPS/Leveling data for the local geoid computations and evaluations are introduced.

3.1 Study Area

The geography of Colorado has a mixed and diverse structure. It is surrounded by high mountains, vast plains, canyons, and rugged terrain. The mountainous area is caused by the Rocky Mountains that lies in the middle of the state. This complex structure makes the area challenging and a good option for experimental studies. In the sense of this study, the rough topography causes an uneven distribution of gravity measurements on terrain. The need of a more homogeneous coverage cause to use of airborne in gravity measurements. To see the effect and the contribution of airborne gravimetry, a study area is selected in Colorado. The study area is defined as $35 < \varphi < 40$ and $250 < \lambda < 258$. The mean orthometric height inside the study area is around 2015 meters, and because of the Rocky Mountains, the maximum orthometric height reaches up to 4321 meters.

3.2 Data

Inside the given limits of the study area, airborne gravity data is distributed over the southern-east corner, and the terrestrial gravity data is spread over a larger area. GNSS/Leveling data sets are sparse and distributed over the whole study area. All of these data sets are provided by The National Geodetic Survey (NGS).

3.2.1 Airborne gravity data

The airborne gravimetry measurements are held by NGS under the Gravity for the Redefinition of the American Vertical Datum (GRAV-D) program. In this program, the airborne measurements are done block by block which is the pre-defined geographic

area for the airborne survey to obtain data lines and additionally cross lines for providing the error statistics. In this thesis, the block Mountain South 05 (MS05) is used. This block covers $131,150\ km^2$ area and includes a part of Colorado, Kansas, New Mexico, Oklahoma, and Texas.

As it is stated before, the study area is limited with Colorado and extended according to the airborne data. The airborne gravity data is distributed over the southern-east corner of the study area, and limited between $35 < \varphi < 39$ and $251 < \lambda < 258$ (see Figure 3.1). There are 49 lines along the West-East direction, and 7 lines along the North-South direction. The spacing between the lines along the West-East direction is 10 km, and for the cross lines it is around 80 km. The mean flight altitude is around 6186 m where the minimum 5208 m, and the maximum is 7905 m. Basic principles of airborne gravimetry is followed during collecting the airborne gravity data. In Appendix A, these principles are explained. The GPS and the gravity data preprocessing is held by NGS using a program called Inertial Explorer (IE) v8.7. First the GPS-only kinematic data is processed, then the average position accuracy for the data block is obtained. The average horizontal position accuracy is ± 0.052 m and the average vertical position accuracy is ± 0.087 m which corresponds to 95% confidence interval. For the preprocessing of the gravity data, a Gaussian filter with 6-sigma is applied three times to remove the noise carefully. However, some noise still remains in the provided data set. The first provided data set consists 2.5 million points (20 Hz). Because of the biases in the first release, another debiased data set is provided by NGS. The second release consists 283,716 points (1 Hz) is used in this study.

3.2.2 Terrestrial gravity data

The terrestrial data is distributed all over the study area unlike the airborne gravity data set. Especially, this distribution gets dense in the northern parts of the mid-longitude and the west part of the mid-latitude. Around the mountainous area, it can be seen that the observations are held over the plane part of the topography. This gravity data is a collection of multiple survey campaigns, thus the metadata of this gravity data set has missing parts such as the date, the used gravimeter etc. In total, this collection has 59,303 points that is spread over the study area. In the given data, instead of providing the measured gravity, the surface gravity anomalies are given. The cleaning of the

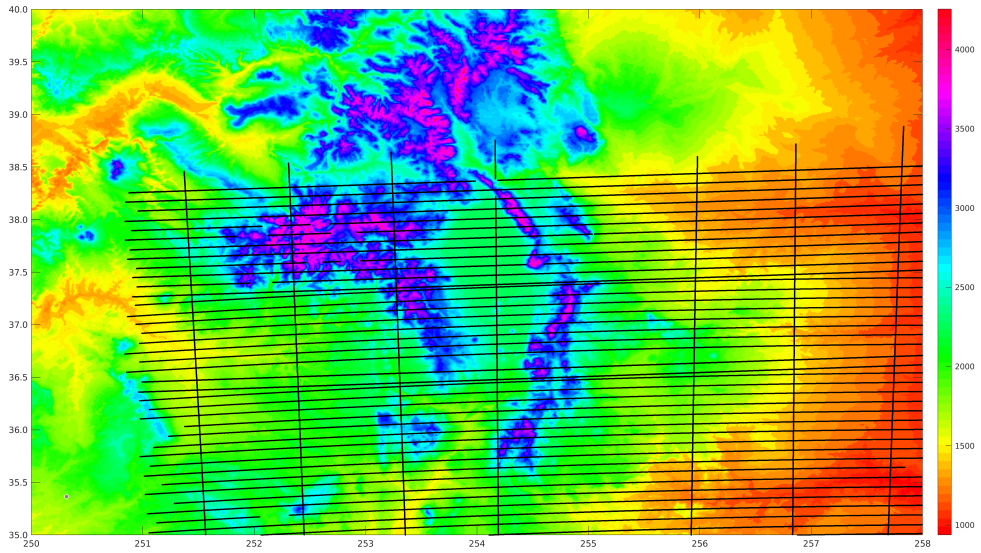

Figure 3.1 : Airborne tracks over the Digital Terrain Model of the study area. Unit is in meters.

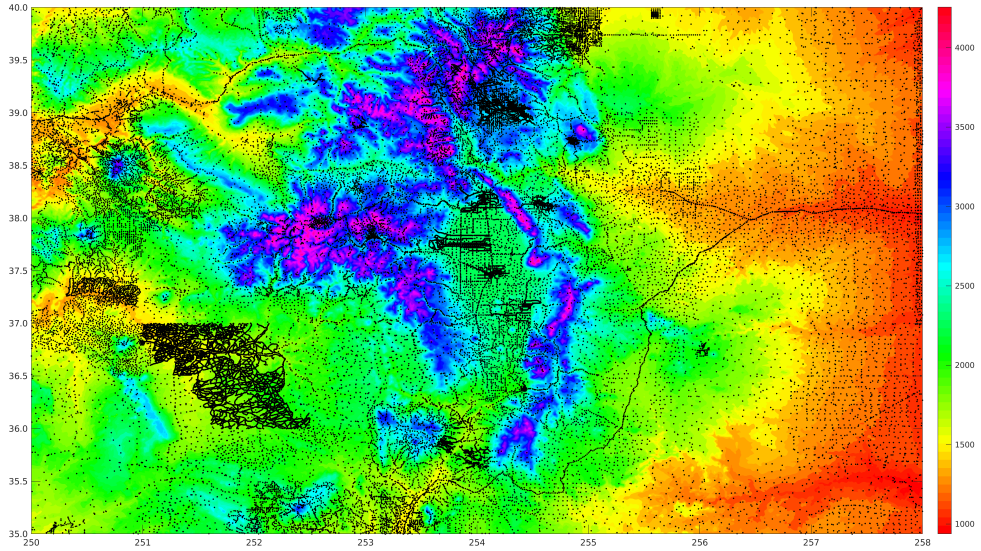

Figure 3.2 : Terrestrial gravity data set on the topography. Unit is in meters.

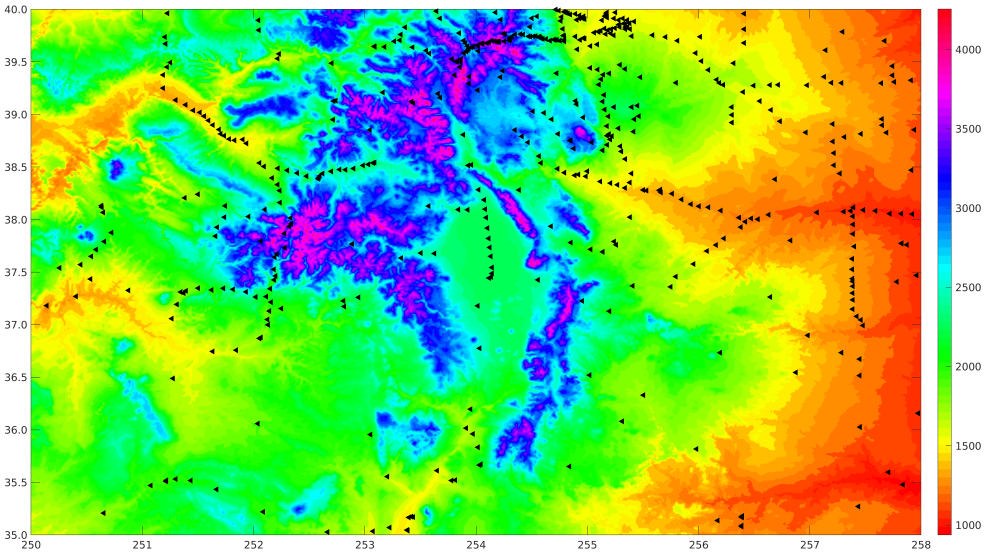

Figure 3.3 : Historical GPS/Leveling data on the topography. Unit is in meters.

terrestrial gravity data is mentioned in the following sections.

3.2.3 GPS/Leveling data

The historical GPS/Leveling data set consists 509 benchmarks that is spread over the study area both from Colorado and the surrounding states. This data set is sparse due to the rough topography, especially around the mid-longitude. 467 benchmarks are from the NGS Integrated Database (IDB) and 42 marks from NGS OPUS-Share Tool (https://www.ngs.noaa.gov/OPUS/). Orthometric height of these GPS/Leveling benchmarks refers to North America Vertical Datum of 1988 (NAVD88). For the geoid validation, 104 benchmarks of this data set remains inside the computation area ($36 < \varphi < 38$ and $251.5 < \lambda < 257$).

3.3 Data Pre-processing and Analysis

The pre-processing of the data sets are carried out in an earlier study within the scope of the International Association of Geodesy (IAG) Joint Working Group 2.2.2 (JWG2.2.2 – "The 1 cm geoid experiment") (Grigoriadis et al., 2020). The pre-processing and the computation of the residuals are summarized below.

Before any computation, possible outliers, blunders and duplicated values need to be determined and removed from the data set. Thus, the terrestrial gravity data set is

examined for duplicated values. In the given data set, 1 duplicated point is detected. As a second step, possible outliers in the data are searched. At the end, 8 points with the same latitude, longitude and orthometric height but different gravity values, less than 0.015 mGal, are deleted and 4 points are regenerated from those values by taking the average. Similar to this, 12 points with the same latitude, longitude and orthometric height with a difference over 0.015 mGal are deleted. 838 points with the same latitude, longitude, different orthometric heights and gravity, 327 points with the same latitude and longitude are deleted. After all, the number of the points is decreased from 58,121 from 59,303.

For airborne data, the main problem is the density of the data. First, the duplicated points are searched. However, it is seen that by down-sampling the data, those duplicated values are removed. Depending on the Nyquist rule, down-sampling is performed by selecting the points 1/5 along the track. Before down-sampling, airborne data is filtered track by track to remove the effect of airborne dynamics. In order to do so, a Butterworth filter with 0.00185 Hz cut-off frequency is used. The cut-off frequency is determined based on the range of observed gravity values in the frequency domain.

The residual gravity anomalies are computed as in Equation 2.40. XGM2016 (Pail et al., 2016) up to d/o 719 is used to compute the contribution of long wavelength. Spherical harmonic combination of Earth's potential from the Earth2014 model from d/o 720 (Hirt and Rexer, 2015) up to d/o 2160 and ERTM2160 (Earth Residual Terrain Modelled-gravity field) (Hirt et al., 2014) up to d/o 96000 for higher degree effects are used to model the short wavelength contribution.

4. NUMERICAL RESULTS

In this chapter, the computation of three different geoid models from residual gravity anomalies by using LSC are given. First, the airborne only model is given. This is followed by terrestrial only and combined model. Finally, the evaluations of these models are given in the last section of this chapter.

4.1 Geoid Computation

Three different quasi-geoid models are computed which are airborne only, terrestrial only and combined. Terrestrial only and combined quasi-geoid computations are carried out to observe the effect and contribution of airborne gravity data on local gravity field modelling.

The residual airborne gravity anomalies at flight altitude are downward continued to the Earth's surface in an earlier study within the scope of the International Association of Geodesy (IAG) Joint Working Group 2.2.2 (JWG2.2.2 – "The 1 cm geoid experiment") (Grigoriadis et al., 2020). Therefore, the given quasi-geoid computations are held by using the obtained residual gravity anomalies from the mentioned study. From now on, the downward continued airborne gravity anomalies on surface of the Earth are mentioned as downward continued airborne gravity anomalies.

As a first step, the empirical covariances of both terrestrial and downward continued airborne residual gravity anomalies are computed in order to determine the model covariance function that is used in LSC for the determination of quasi-geoid. The empirical covariances are computed as in Equation 2.35 by taking the sum of the products of the data that is inside an interval as given in Equation 2.34, where the interval length is selected as 0.03333° (equals to 2 arcminute) for downward continued airborne data, based on its grid resolution. For surface gravity anomalies, the interval is selected as 0.025°, which equals to 1.5 arcminute, according to distribution of the terrestrial data set. If the downward continued airborne data had 1 arcminute resolution, the step for the evaluation could be taken as different than 2 arcminutes.

The computation of the empirical covariances are carried out by using the program EMPCOV which is one of the developed softwares inside the GRAVSOFT package.

Normally, different covariance models should be computed for each data set based on their empirical covariances. However, as it is seen in Figure 4.1, the empirical covariances of surface (black marks) and downward continued airborne gravity anomalies on the Earth's surface (blue marks) are in an agreement. Therefore, a covariance model that fits to the empirical covariances of both data sets is computed by using COVFIT (one of the softwares inside the GRAVSOFT package). Additionally, this agreement in the empirical covariances shows that downward continuation process is successful, and those two data sets are consistent. Therefore, the airborne gravity anomalies on the Earth's surface can be used in the geoid computation.

Some parameters (e.g. depth of the Bjerhammar sphere, variance of the data , error degree variances and the expansion degree of them) have to be determined to find a covariance function. Since one possible solution to determination of parameters is trial and error, different parameters are tested to find the best fitting model to the empirical values. The tested parameters are given in the Table 4.1.

Additionally, it is seen that in Grigoriadis et al. (2020), the cross-covariances have an off-set. Thus, the error-degree variances are computed again based on the assumption that it might be related to error-degree variances,

$$\sigma_{\varepsilon}^{2} = \left(\frac{GM}{R^{2}}\right)^{2} (n-1)^{2} \sum_{m=0}^{n} \left(d_{C_{nm}}^{2} + d_{S_{nm}}^{2}\right) \tag{4.1}$$

where $d_{C_{nm}}$ and $d_{S_{nm}}$ are the standard errors of the GGM, in our case it is XGM2016.

In the computation of covariance function, the second model of the degree-variances is used (Tscherning and Rapp, 1974) which is given as

$$\sigma_{n}^{2} = \frac{A}{(n-1)(n-2)(n+B)} \tag{4.2}$$

where A and B are constants to be defined. In practice, A is taken as the variance of the data (C_0). As it is given in Table 4.1, different values are also tried for this parameter in order to compute a covariance function that fits to empirical values of both data sets.

Additionally, the mean topographic height is taken as 2000 m for the computation of model covariances of gravity anomalies (see Section 3.1), since it is stated that

Table 4.1 : Tested parameters (variance of the gravity anomalies, depth of the Bjerhammar sphere, and the error degree variances up to N with scale factor 0.05) for the computation of model covariance based on empirical covariances of both terrestrial and downward continued airborne data.

	C_0 (mGal^2)	R_B (km)	N (d/o)
Test-1	70	-3.0	700
Test-2	70	-3.0	690
Test-3	100	-3.0	700
Test-4	100	-3.0	690

the covariance function refers to the mean topographic height of the area (Sansò and Sideris, 2013).

Among these trials, best fit is obtained by parameters used in Test-4. The covariance values for each test can be seen in Table B.1. The empirical covariances of both data sets and the model covariance values reach to zero around the same spherical distance, around 0.125°, as it is seen Figure 4.1, and this can be checked for the models obtained from other tests (see Table B.1). As it is seen in Table B.1, covariance models obtained from Test-1, Test-2, and Test-3 reach to zero around 0.150°, while for Test-4 it is 0.125°.

As it is seen in Figure 4.1, the model at 2000 m and the empirical covariance values are in a good agreement. Thus, these parameters are used in LSC for the further computations, i.e. combining terrestrial and downward continued airborne data on the surface, computation of airborne only, terrestrial only and combined quasi-geoid models. As a next step, the establishment of the normal equations, solution of those equations and predictions (see Equation 2.24 and 2.53) are carried out with the parameters of Test-4 by using GEOCOLIGS which is a program developed at PoliMi. For the combination of airborne and terrestrial data, the related equations are 2.24 and 2.38. For the estimation of height anomalies from residuals, the relation is defined by Equation 2.39 and 2.53. The number of observations is directly proportional to the system of equations to be solved. Therefore, the program is re-compiled according to the maximum number of observations.

All quasi-geoid computations are performed on a grid with 2 arcmin resolution and also on sparse historical 104 GPS/Leveling points inside the computation area. Then, the estimated residual height anomalies are restored with the same models and parameters

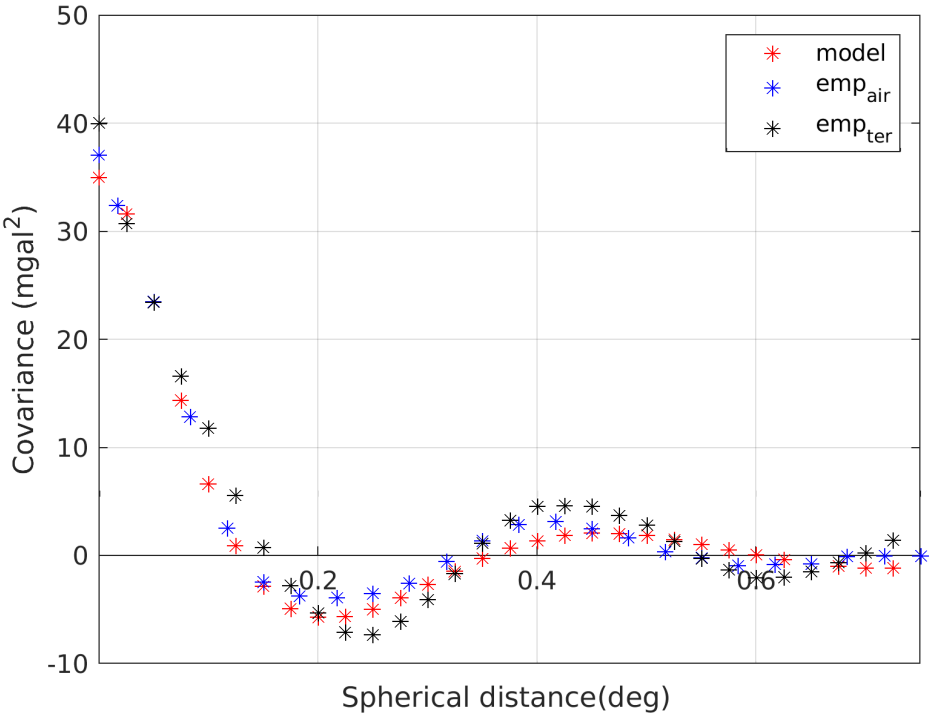

Figure 4.1 : Covariance model at 2000 m (red) and the empirical covariances of downward continued (blue) airborne and surface residual gravity anomalies (black).

as in remove step, only the functional is changed from gravity anomalies to height anomalies (see Equation 2.47). The evaluation of these solutions are performed on the GPS/Leveling points and restricted to a common area with the combined solution in order to have a better comparison of the different solutions. Inside this common area, there are 87 historical GPS/Leveling points. The results of these quasi-geoid solutions are given, in the following order, airborne only, terrestrial only and combined, under the Sections 4.1.1, 4.1.2 and 4.1.3. The evaluation of these models are mentioned completely under another section (see Section 4.2).

4.1.1 Airborne only solution

The full computation scheme for airborne solution, including downward continuation, can be seen in Figure 2.6. By using the parameters for Test-4 that is given in Table 4.1, LSC is performed to estimate the residual height anomalies from downward continued residual airborne gravity anomalies. The estimated residual height anomalies present a rapidly changing surface, especially around the mid-longitude of the computation area as seen in Figure 4.2. The rapidly changing surface is a result of the rough topography, since the high mountains are seen in this part of the computation area (see Figure 3.1). Therefore, we can state that the RTM effect for the airborne data is not fully sufficient to represent the topography. Additionally, some anomalies reach to -15 cm are seen between 36.6° - 36.8° N and 254° - 255° E in Figure 4.2. This is related to lack of data around this area. As it is seen in Figure 3.1, the distance between two airborne tracks in the stated area is larger than the usual distance. The residual height anomalies are restored by using Equation 2.47 as it is mentioned in the section above. By restoring the long and short frequency components, the airborne only quasi-geoid model is computed as seen in Figure 4.3. The statistics of the estimated residual and the restored height anomalies are given in Table 4.2.

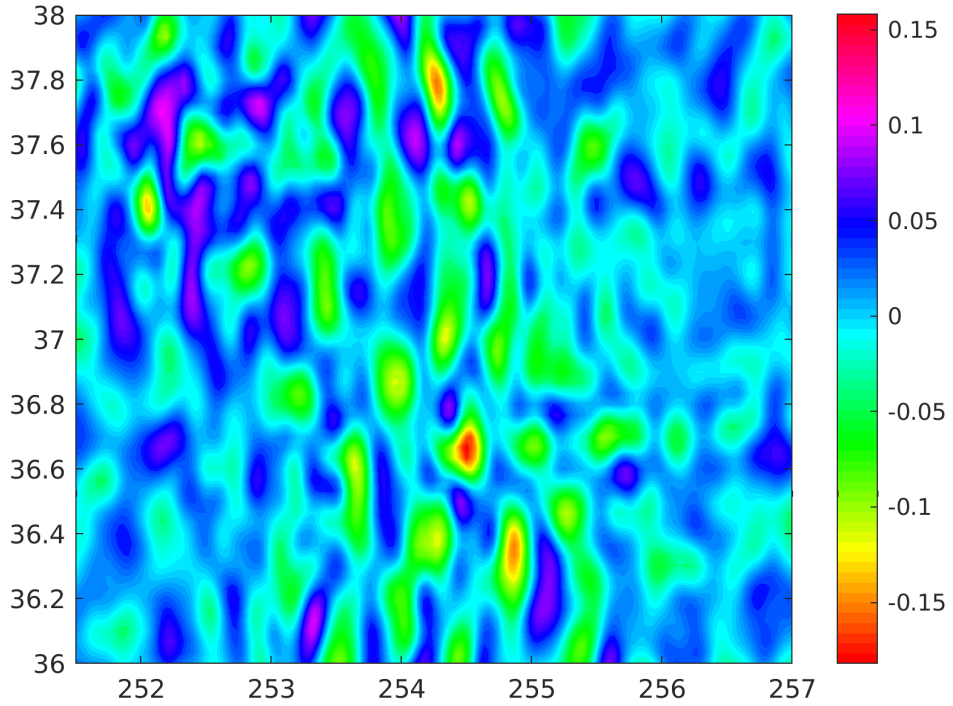

Figure 4.2 : The computed residual height anomalies from residual downward continued gravity anomalies. Unit is meters.

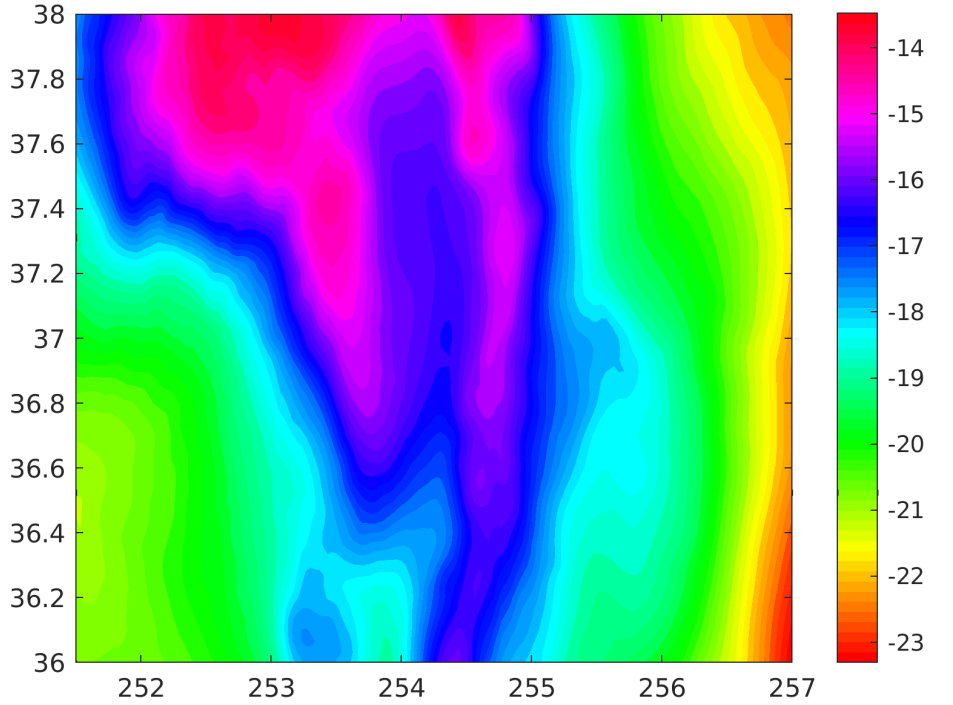

Figure 4.3 : Airborne only quasi-geoid model. Unit is meters.

4.1.2 Terrestrial only solution

The same steps are also followed for terrestrial only solution. The general scheme can be seen in Figure 2.5. The residual height anomalies are estimated by using the sparse residual surface gravity data which is given in Figure 4.4.

In Figure 4.5, the estimated residual height anomalies are given. As in airborne only residual height anomalies, the surface changes very quickly again around the mid-longitude for the estimated terrestrial only height anomalies. However, those changes are smaller compared to airborne only solution.

Residual height anomalies are seen to be peaked in the area between 37.4° - 37.8° N and 252° - 253° E. As one can see in Figure 3.2, there is no surface data inside the mentioned limits. Therefore, lack of data causes such rapidly changing anomalies. In contrast to Figure 4.2, the residual height anomalies present a good residual surface in the plain part of topography as seen in Figure 4.5.

The terrestrial only quasi-geoid model is given in Figure 4.6. This terrestrial only model shares some similar features which are seen in airborne only quasi-geoid model such as rapid change towards the high mountains. The statistics of the residual and restored height anomalies can be found in Table 4.2.

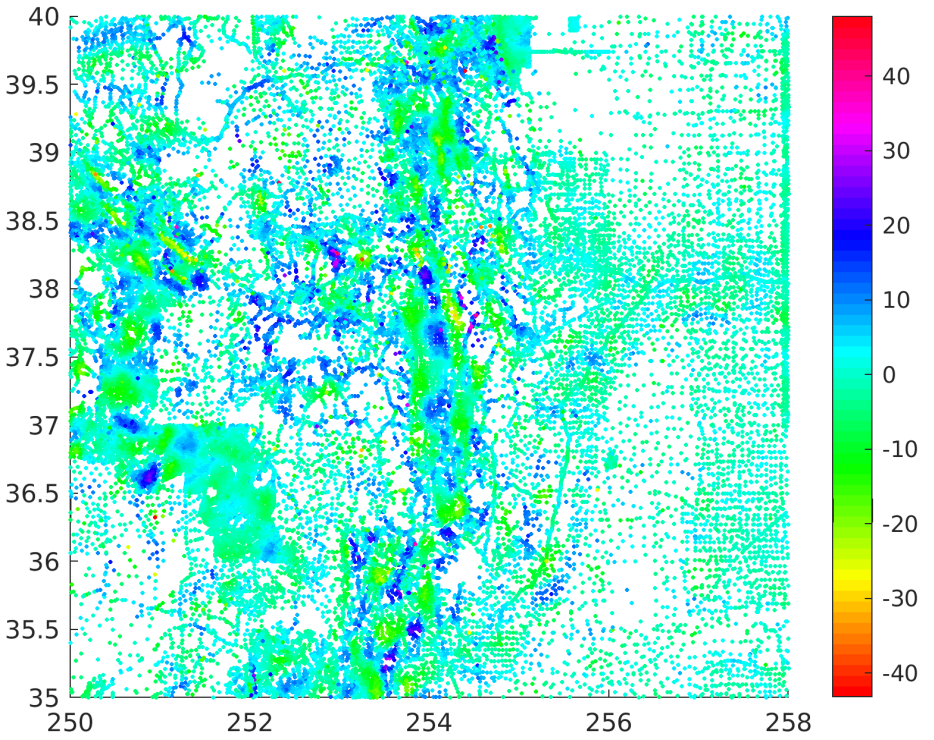

Figure 4.4 : Residual surface gravity anomalies. Unit is in mGal.

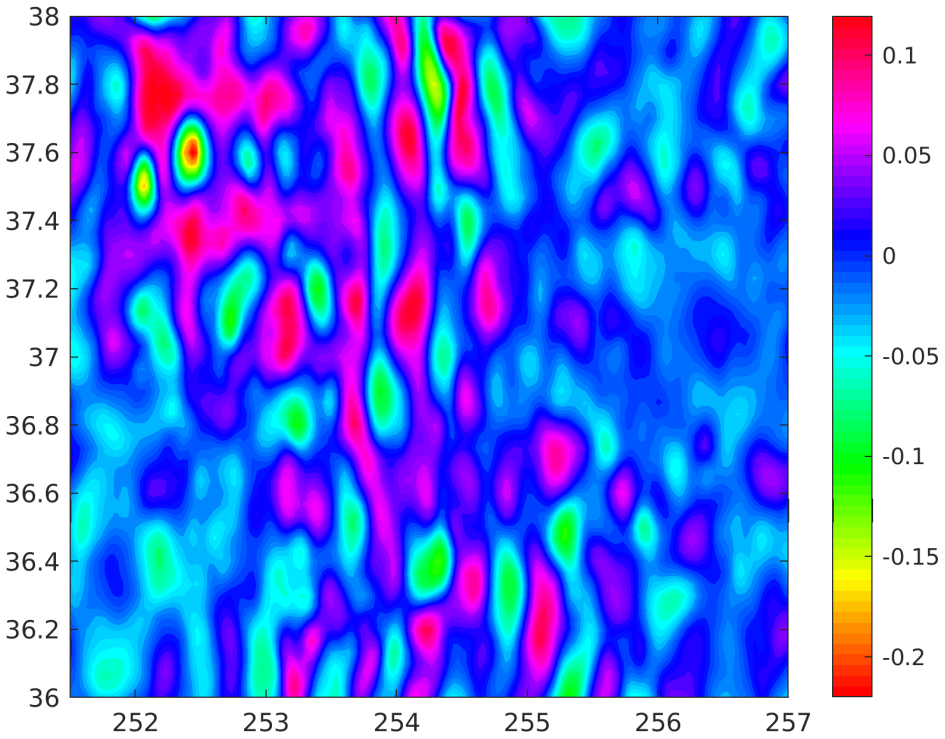

Figure 4.5 : The terrestrial residual height anomalies. Unit is in meters.

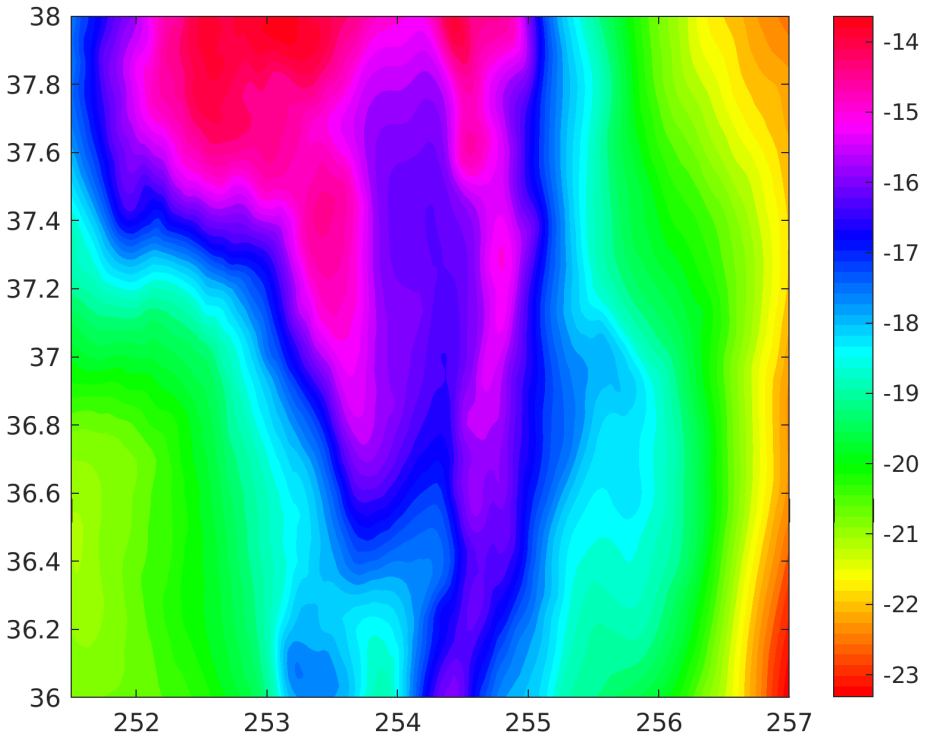

Figure 4.6 : Terrestrial only quasi-geoid model. Unit is in meters.

4.1.3 Combined solution

Before combining the residual surface and downward continued airborne gravity anomalies, a data selection is performed for terrestrial data set based on the difference between residual surface gravity anomalies and downward continued residuals. The selection of thresholds for this procedure is done by following 2.5σ principle. In this procedure, σ corresponds to 4.96 mGal for difference with downward continued residuals. The terrestrial gravity points which have differences with the downward continued residuals over ± 12.5 mGal are removed for combination with downward continued airborne residuals. This corresponds to removal of 547 points from terrestrial data set.

After data selection, the two data sets are merged in the area 36° - 38° N and 251.5° - 257° E over $2' \times 2'$ grid according to Equation 2.52 by GEOCOLIGS using the same covariance parameters as it is stated above. As in airborne and terrestrial only solutions, same grid resolutions is selected by considering the data distribution. In this way, any possible oversampling issue is avoided, and the necessary amount of

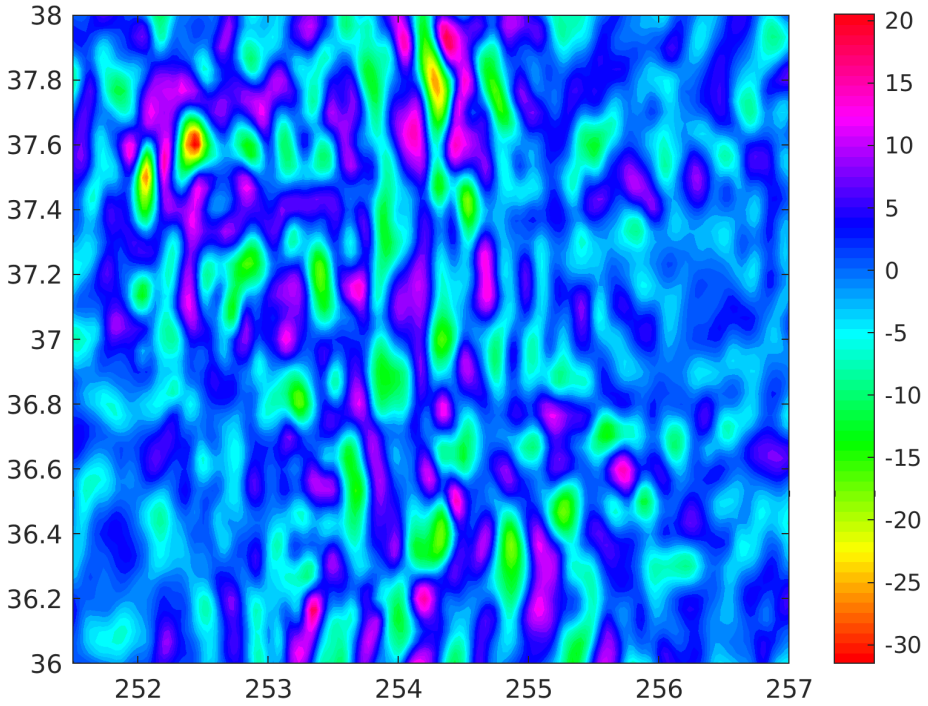

Figure 4.7 : The combined residual gravity anomalies over $2' \times 2'$ grid. Unit is in mGal.

points for the quasi-geoid computations are obtained. The combined residual gravity anomalies are given in Figure 4.7. The lack of data still causes some discrepancies in the area between 37.4° - 37.8° N and 252° - 253° E for both combined residual gravity (Figure 4.7) and height anomalies (Figure 4.8). But the effect is slightly reduced.

The prediction of height anomalies are performed in a smaller area to avoid the edge effects. The limits of the new computation area are 36.2° - 37.8° N and 251.8° - 256.8° E.

As seen in Figure 4.8, it gives a smooth surface which is mostly centered around zero. Combining airborne and terrestrial data decreases the discrepancies which are caused by the lack of data and the effect of the topography. Therefore, the combined solution presents a smoother residual surface. In Figure 4.9, the combined quasi-geoid is given. As in Figure 4.3 and 4.6, similar features are seen for the combined model as well.

The statistics of residual and restored height anomalies are given in Table 4.2 in order to see the statistical variations of the computed quasi-geoid models. More or less all solutions have similar ranges. Additionally, another statistic is given in Table 4.3 to see

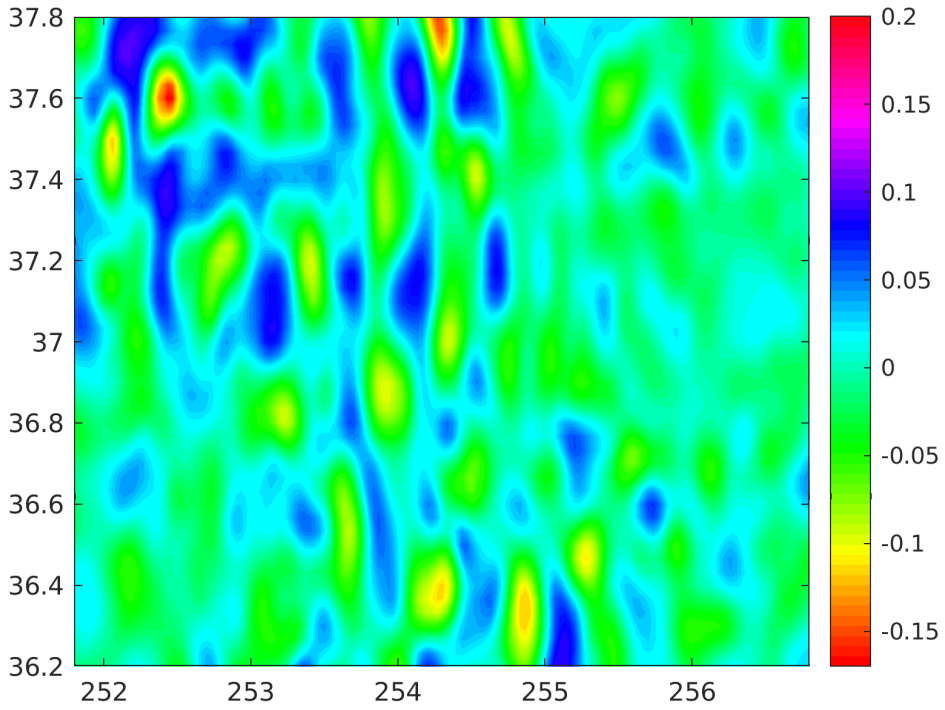

Figure 4.8 : The combined residual height anomalies over $2' \times 2'$ grid. Unit is in meters.

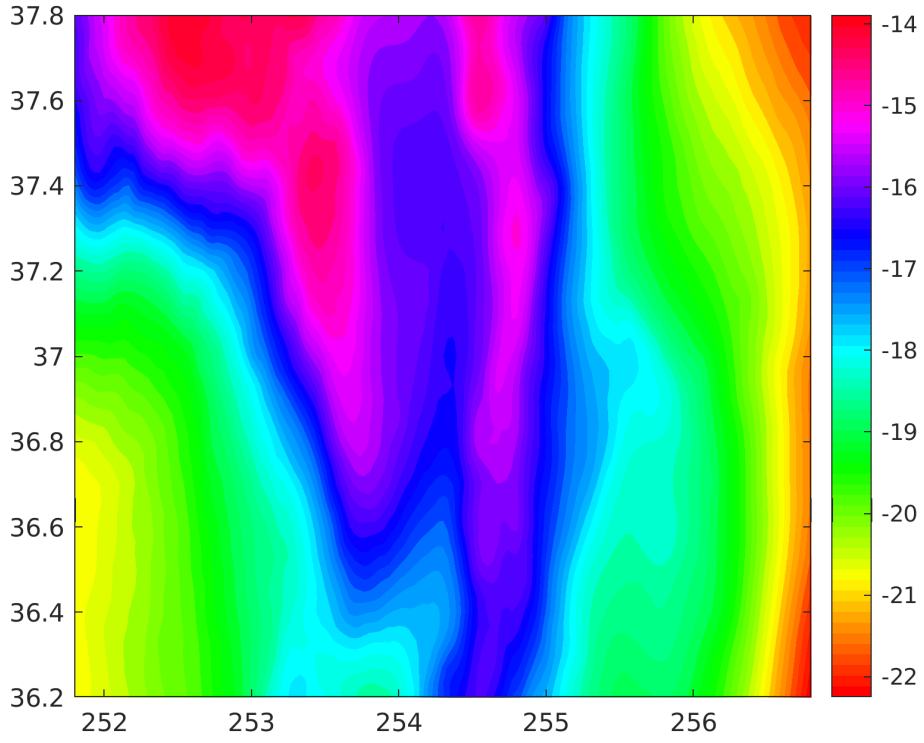

Figure 4.9 : The combined quasi-geoid model over $2' \times 2'$ grid. Unit is in meters.

Table 4.2 : Statistics of the residual height anomalies(ζ_{RES}) and computed quasi-geoid models (ζ) coming from airborne only, terrestrial only, and combined solutions. Unit is in meters.

		Min	Max	Mean	Std
Air	ζ_{RES}	-0.182	0.110	0.003	0.036
	ζ	-23.304	-13.476	-17.955	2.204
Ter	ζ_{RES}	-0.220	0.126	0.003	0.039
	ζ	-23.317	-13.451	-17.954	2.221
Comb	ζ_{RES}	-0.166	0.106	0.001	0.035
	ζ	-22.247	-13.899	-17.721	1.971

Table 4.3 : Height anomaly differences between terrestrial only model and the others over $2' \times 2'$ grid. Unit is in meters.

	Min	Max	Mean	Std
$\zeta_{ter} - \zeta_{air}$	-0.149	0.229	0.001	0.032
$\zeta_{ter} - \zeta_{comb}$	-0.071	0.115	0.003	0.017

how much the airborne only and combined model vary from the terrestrial only model. The visualisation of these differences are given in Figure 4.10 and 4.11.

In Figure 4.10 and 4.11, the major differences are seen in the mountainous area. As it is stated before, this can be related either to the RTM effect of the airborne data due to inconsistencies around rough topographic features, or the quality of the terrestrial gravity data set.

Once again, the indirect effect of the gap between two airborne tracks around 36.6° N (see also Figure 3.1) on downward continued airborne gravity anomalies causes anomalies along this latitude which can be seen clearly in Figure 4.10. Additionally, some of the discrepancies (e.g. northern part of the area) are a result of the lack of data in terrestrial data set (see Figure 3.2). From here, one can draw a conclusion that the airborne data refine the area where the terrestrial data shows weakness. Aside from the discrepancies, airborne only solution is comparable to terrestrial only model. Therefore, the difference between those models is centered around zero (see Table 4.3).

In contrast to height anomaly differences between airborne and terrestrial only models, difference with combined model presents a smoother surface (see Figure 4.11). Especially, it is seen that the lack of data problems, which are mentioned above, are slightly reduced by combining surface and downward continued airborne gravity anomalies.

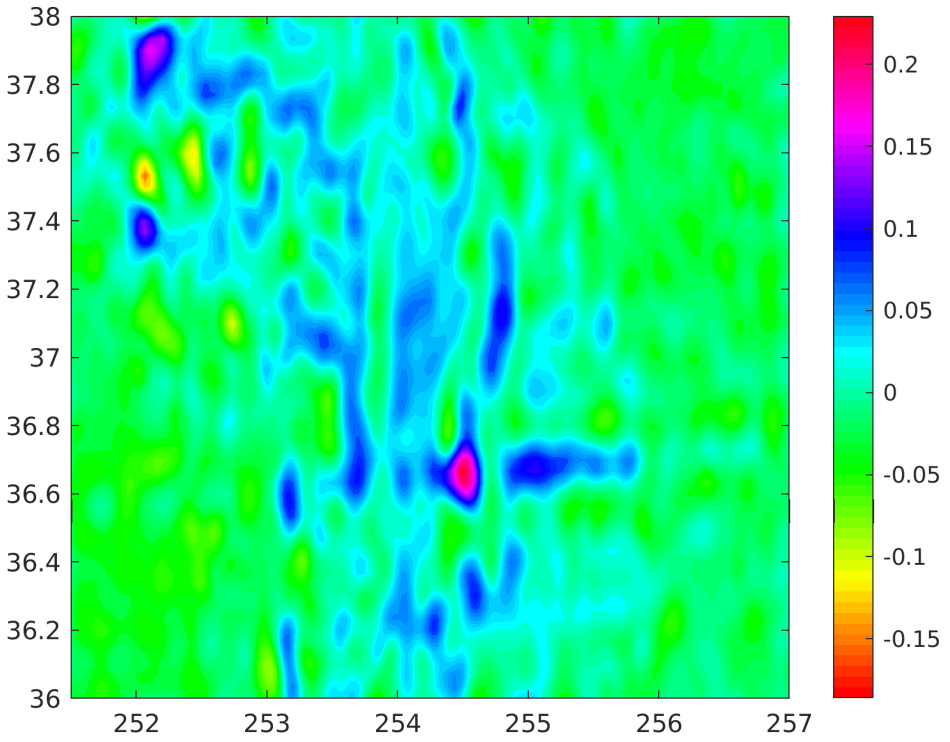

Figure 4.10 : Height anomaly differences between terrestrial only and airborne only model over $2' \times 2'$ grid. Unit is in meters.

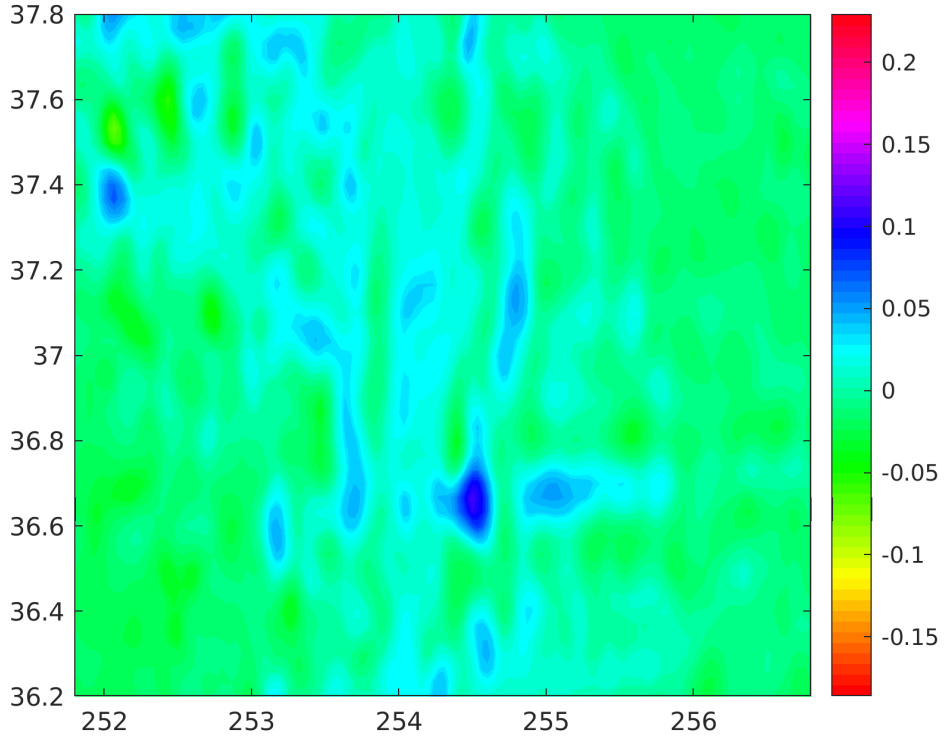

Figure 4.11 : Height anomaly differences between terrestrial only and combined model over $2' \times 2'$ grid. Unit is in meters.

4.2 Evaluation of the Models

The models presented above are tested over the sparse GPS/Leveling points inside the computation area. Inside this area, there are 104 sparse GPS/Leveling points. However, the computation area for the combined model is slightly smaller than the others. Thus, the area limits of the combined models are selected as a common area for the model validations and comparisons. The common area includes 87 sparse points. Since the geoid heights can be derived from the GPS/Leveling data as in

$$h - H = N \tag{4.3}$$

where h is the ellipsoidal, H is the orthometric, and N is the geoid height, it is more convenient to test the quasi-geoid models by converting the computed height anomalies to geoid heights. In order to do so, the height anomaly values which are computed on these sparse 87 GPS/Leveling points are converted to geoid heights by using the following equation

$$N - \zeta \cong \frac{\Delta g_B}{\bar{\gamma}} H \tag{4.4}$$

where $\bar{\gamma}$ is the mean normal gravity along the plumb line between the surface of the Earth and quasi-geoid, and H is the orthometric height, and Δg_B which is the Bouger anomaly is computed as

$$\Delta g_B = \Delta g_{FAA} - 0.1119 \times H \tag{4.5}$$

where Δg_{FAA} is the free-air gravity anomalies. After the conversion of height anomalies, the obtained geoid heights are evaluated over the sparse GPS/Leveling points. Initial statistics of the difference between geoid heights, which are obtained by converting the computed height anomalies, and the geoid heights derived from GPS/Leveling data are given in Table 4.4. To eliminate the effects of systematic errors and datum inconsistencies, corrector surface fitting is applied as (Fotopoulos, 2003)

$$\Delta N = N_{GPS/Lev} - N_{model} = a^T \mathbf{x} + \varepsilon \tag{4.6}$$

where a is the known coefficients, x is the unknown parameters and ε is the random noise. For corrector surface fitting, a 4-parameter Helmert Similarity Trasformation is performed which is given as

$$a_i = [1 \quad \cos\phi_i \cos\lambda_i \quad \cos\phi_i \sin\lambda_i \quad \sin\phi_i] \tag{4.7}$$

Table 4.4 : Statistics over sparse GPS/Leveling points of the final geoid heights obtained by converting the height anomalies. Unit is in meters.

		Min	Max	Mean	STD	RMSE
Before-fit	Air	0.875	1.182	1.009	0.064	1.011
	Ter	0.881	1.192	1.008	0.066	1.010
	Comb	0.879	1.185	1.007	0.063	1.008
After-fit	Air	-0.160	0.100	0.000	0.049	0.049
	Ter	-0.127	0.108	0.000	0.048	0.048
	Comb	-0.131	0.102	0.000	0.047	0.047

So-called after-fit statistics are given in Table 4.4. It can be stated that the best solution is obtained from the combined model. This is the result of overcoming the lack of data problem by forming a third and densely distributed data set. Especially, airborne data has a major impact in covering the northern and mountainous part of the computation area where the distribution of the terrestrial data is weak. Nevertheless, the worst result belongs to the terrestrial only model. This can be explained by the quality of the terrestrial data set.

In Figure 4.12, variations of the geoid heights which are computed by converting the height anomalies at these 87 sparse GPS/Leveling points from geoid heights derived from GPS/Leveling are given. Higher differences are seen in the area between 251° - 252 ° E. This might be related to rapid change of the topography which can have an effect on accuracy of the measurements. Although, the topography changes are slightly smoother than in the mentioned area, same explanation also applies to the middle part of the area.

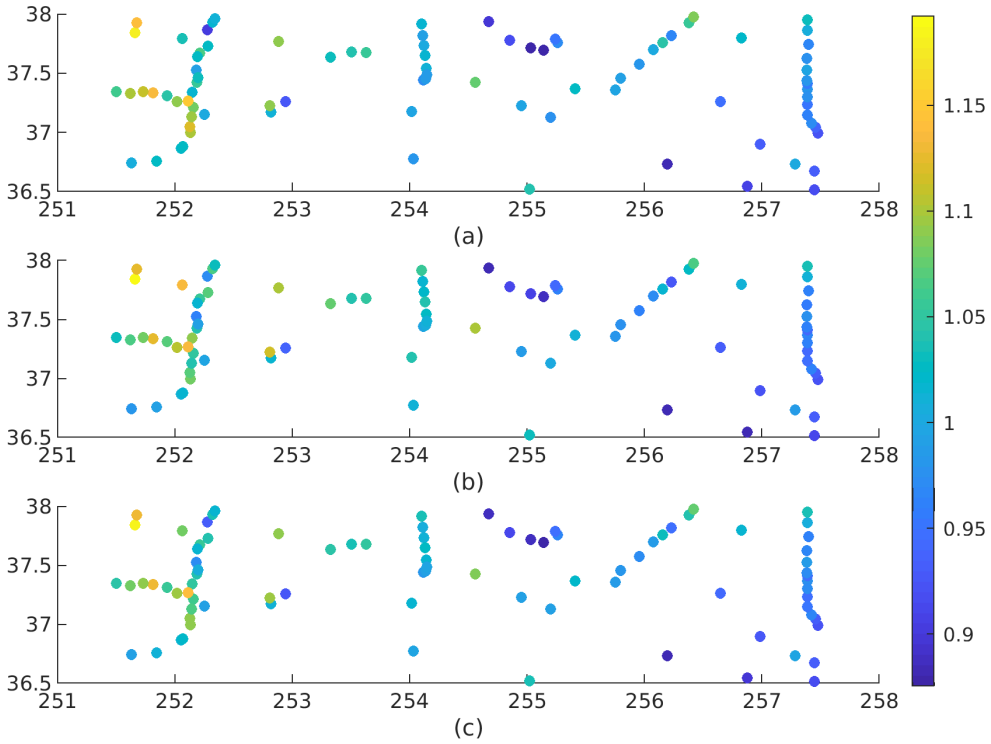

Figure 4.12 : Differences between $N_{GPS/Lev}$ and N_{model} at 87 points. (a) Airborne only, (b) Terrestrial only, (c) Combined. Unit is meters.

5. CONCLUSION AND DISCUSSION

In this final chapter, a detailed explanation and conclusions of the obtained results are given. Based on the outcomes of this study, a number of recommendations are given for the further experiments and studies in airborne gravimetry.

The aim of this dissertation is to investigate the contribution of the airborne gravimetry in order to determinate an accurate geoid/quasi-geoid model of Colorado which requires a dense and homogeneously distributed gravity data. Thus, in this study both terrestrial and airborne gravity data are used. A dense and homogeneously distributed gravity data set is formed by combining terrestrial and airborne gravity data sets in order to obtain an accurate quasi-geoid model. However, the characteristic difference of these two data sets brings in some problems with itself, i.e. resolution, coverage, data handling, topographic reductions. Therefore, it is really important to understand their characteristics to merge them and obtain a successful gravity model.

Three different quasi-geoid models are computed based on the used data sets to see the effect of the mentioned characteristics. These are:

- Airborne only
- Terrestrial only
- Combined

These models are computed by applying LSC to the residual gravity anomalies (see Chapter 2 and 4). The motivation of using LSC in computations can be listed as

- Different data types can be used together in order to estimate the height anomalies (or any functional of the disturbing potential).
- Gridded data is not required. Sparse data can be used in the computations.
- It provides a good adaptation of the data through empirical covariances, which makes LSC an optimal method for the estimation of height anomalies.

The Remove-Restore technique is used to obtain the residuals used in the quasi-geoid computations. XGM2016 up to d/o 719 is applied to remove the low frequency part of the gravity signal, where the high frequency part is modelled by combining spherical harmonic expansion of Earth2014 up to d/o 2160 and ERTM2160 up to d/o 96000. LSC is applied to these three data sets to compute residual height anomalies which are later evaluated over 87 historical sparse GPS/Leveling points by restoring the removed effects and converting the height anomalies to geoid undulations. As a result of this evaluation, following outcomes are obtained:

- Combined solution provides the best results over the historical sparse GPS/Leveling points as 6.3 cm (see Table 4.4) by means of standard deviation of geoid height differences. This is a result of using a dense and better distributed data set. The combination of residual surface and airborne gravity anomalies resolves the lack of data problems. Specially, airborne data shows the expected contribution in the areas where no terrestrial gravity data is available.

- Airborne only solution has a slightly improved accuracy compare to the terrestrial only model. This result can be enhanced by refining the long and short wavelength contribution, especially the RTM effect, since main discrepancies between airborne only and terrestrial only model (see Figure 4.10) are seen in the mountainous area. The current topography related models might be insufficient to compute the RTM effect of the high resolution airborne data. In this context, it has to be reminded that the first released data set has 20 Hz (0.05 sec) resolution which is later resampled to 1 Hz (1 sec). Therefore, either residuals or the RTM effect might need to be filtered along the airborne track (Forsberg and Olesen, 2010).

- The historical sparse GPS/Leveling points are not precise enough to test the results for under 5-6 cm. Thus, the results should be tested over GSVS line which is measured on purpose of providing a more precise test data.

- In Grigoriadis et al. (2020), three different models by using three different methods (e.g. FFT, LSC, WLSC) are presented. However, the worst results over historical sparse GPS/Leveling points belong to the models computed by LSC. The solutions obtained by LSC over historical sparse GPS/Leveling points give 6.4 cm for airborne only model, 7.7 cm for terrestrial only, and 7.4 cm for combined model

in the mentioned study. Due to an off-set in the cross covariances, the estimated residual height anomalies are deflected from the ones coming from the WLSC (Window LSC). In this thesis, the off-set seen in the cross-covariances is removed by changing the error degree variances. In this way, the LSC solutions in Grigoriadis et al. (2020) are enhanced, especially terrestrial only and combined model show an improvement around 1 cm. As it is given in Table 4.4, the results over historical sparse GPS/Leveling points give 6.4 cm for airborne only model, 6.6 cm for terrestrial only, and 6.3 cm for combined model by means of standard deviation of geoid height differences.

- The studies under the context of GRAV-D project show that the airborne gravity data improves the gravity field representation in many parts of the U.S., especially in Iowa (Wang et al., 2017) up to 1 cm, over the Great Lakes region (Li et al., 2016) up to 1-3 cm, and in the regional scale of the U.S. (Smith et al., 2013) up to 1 cm improvement in the accuracy of the geoid models. However, the validation of these models are performed by using the Geoid Slope Validation Survey data sets. Those models show better improvements which reach up to 3 cm, since GSVS data sets are more reliable than the historical GPS/Leveling data sets. In McCubbine et al. (2018), high differences which reach to 12 cm are seen between airborne included and not included height anomalies. By testing the models on GPS/Leveling points, it is observed that airborne data has a contribution in the gravimetric quasi-geoid of New Zealand (McCubbine et al., 2018). Aside from the contribution of airborne data, a similar conclusion related to RTM effect of the airborne data is mentioned in Barzaghi et al. (2015) for the discrepancies seen between airborne and terrestrial data set around the mountainous part of Italy.

REFERENCES

Barzaghi, R., Albertella, A., Carrion, D., Barthelmes, F., Petrovic, S., and Scheinert, M.(2015). Testing airborne gravity data in the large-scale area of italy and adjacent seas. In *IGFS 2014*, pages 39–44. Springer.

Forsberg, R. (1984). A study of terrain reductions, density anomalies and geophysical inversion methods in gravity field modelling. Technical report, Ohio State Univ Columbus Dept Of Geodetic Science and Surveying.

Forsberg, R., Olesen, A., Keller, K., Møller, M., Gidskehaug, A., and Solheim, D. (2001). Airborne gravity and geoid surveys in the Arctic and Baltic seas. In *Proceedings of international symposium on kinematic systems in geodesy, geomatics and navigation (KIS-2001), Banff*, pages 586–593.

Forsberg, R., Olesen, A., Munkhtsetseg, D., and Amarzaya, B. (2007). Downward continuation and geoid determination in Mongolia from airborne and surface gravimetry and srtm topography. In *2007 International Forum on Strategic Technology*, pages 470–475. IEEE.

Forsberg, R. and Olesen, A. V. (2010). Airborne gravity field determination. In *Sciences of geodesy-I*, pages 83–104. Springer.

Forsberg, R. and Tscherning, C. (1997). Topographic effects in gravity field modelling for bvp. In *Geodetic boundary value problems in view of the one centimeter geoid*, pages 239–272. Springer.

Fotopoulos, G. (2003). *An analysis on the optimal combination of geoid, orthometric and ellipsoidal height data*. University of Calgary, Department of Geomatics Engineering.

Grigoriadis, V. N., Vergos, G. S., Barzaghi, R., Carrion, D., and Koç, O. (2020). Collocation and fft-based geoid estimation within the colorado 1 cm geoid experiment. *Journal of Geodesy*, Under Review.

Heck, B. (1997). Formulation and linearization of boundary value problems: from observables to a mathematical model. In *Geodetic boundary value problems in view of the one centimeter geoid*, pages 119–160. Springer.

Heiskanen, W. A. and Moritz, H. (1967). Physical geodesy. *San Francisco, WH Freeman [1967]*.

Hirt, C., Bucha, B., Yang, M., and Kuhn, M. (2019). A numerical study of residual terrain modelling (rtm) techniques and the harmonic correction using ultra-high-degree spectral gravity modelling. *Journal of Geodesy*, 93(9):1469–1486.

Hirt, C., Kuhn, M., Claessens, S., Pail, R., Seitz, K., and Gruber, T. (2014). Study of the earth s short-scale gravity field using the ertm2160 gravity model. *Computers & Geosciences*, 73:71–80.

Hirt, C. and Rexer, M. (2015). Earth2014: 1 arc-min shape, topography, bedrock and ice-sheet models–available as gridded data and degree-10,800 spherical harmonics. *International Journal of Applied Earth Observation and Geoinformation*, 39:103–112.

Hofmann-Wellenhof, B. and Moritz, H. (2006). *Physical geodesy*. Springer Science & Business Media.

Hvidegaard, S. M. and Forsberg, R. (2002). Sea-ice thickness from airborne laser altimetry over the arctic ocean north of greenland. *Geophysical Research Letters*, 29(20):13–1.

Hwang, C., Hsiao, Y.-S., Shih, H.-C., Yang, M., Chen, K.-H., Forsberg, R., and Olesen, A. V. (2007). Geodetic and geophysical results from a taiwan airborne gravity survey: Data reduction and accuracy assessment. *Journal of Geophysical Research: Solid Earth*, 112(B4).

Kern, M. and Schwarz, K. (2002). A comparison of direct and indirect numerical methods for the downward continuation of airborne gravity data. In *Vistas for Geodesy in the New Millennium*, pages 242–247. Springer.

Kern, M., Schwarz, K., and Sneeuw, N. (2003). A study on the combination of satellite, airborne, and terrestrial gravity data. *Journal of geodesy*, 77(3-4):217–225.

Li, X., Crowley, J. W., Holmes, S. A., and Wang, Y.-M. (2016). The contribution of the grav-d airborne gravity to geoid determination in the great lakes region. *Geophysical Research Letters*, 43(9):4358–4365.

Li, X. and Huang, J. (2019). Downward continuation methods of airborne gravity data and their impacts on local geoid modeling. In *Geophysical Research Abstracts*, volume 21.

McCubbine, J., Amos, M., Tontini, F., Smith, E., Winefied, R., Stagpoole, V., and Featherstone, W. (2018). The new zealand gravimetric quasigeoid model 2017 that incorporates nationwide airborne gravimetry. *Journal of Geodesy*, 92(8):923–937.

McOwen, R. C. (2004). *Partial differential equations: methods and applications*. .

Moritz, H. (1980). Advanced physical geodesy. *Advances in Planetary Geology*.

Müller, F. and Mayer-Gürr, T. (2005). Comparison of downward continuation methods of airborne gravimetry data. In *A Window on the Future of Geodesy*, pages 254–258. Springer.

Pail, R., Fecher, T., Barnes, D., Factor, J., Holmes, S., Gruber, T., and Zingerle, P. (2016). The experimental gravity field model xgm2016. In *International Symposium on Gravity, Geoid and Height System 2016-1st Joint Commission 2 and IGFS Meeting*.

Rebhan, H., Aguirre, M., and Johannessen, J. (2000). The gravity field and steady-state ocean circulation explorer mission-goce. *ESA Earth Observation Quarterly*, 66:6–11.

Reigber, C., Schwintzer, P., and Lühr, H. (1999). The champ geopotential mission. *Boll. Geof. Teor. Appl*, 40:285–289.

Sansò, F. and Sideris, M. G. (2013). *Geoid determination: theory and methods*. Springer Science & Business Media.

Sjöberg, L. E. (2011). Geoid determination by spectral combination of an earth gravitational model with airborne and terrestrial gravimetry—a theoretical study. *Studia Geophysica et Geodaetica*, 55(4):579.

Smith, D. A., Holmes, S. A., Li, X., Guillaume, S., Wang, Y. M., Bürki, B., Roman, D. R., and Damiani, T. M. (2013). Confirming regional 1 cm differential geoid accuracy from airborne gravimetry: the geoid slope validation survey of 2011. *Journal of geodesy*, 87(10-12):885–907.

Studinger, M., Bell, R., and Frearson, N. (2008). Comparison of airgrav and gt-1a airborne gravimeters for research applications. *Geophysics*, 73(6):I51–I61.

Tscherning, C., Rubek, F., and Forsberg, R. (1998). Combining airborne and ground gravity using collocation. In *Geodesy on the Move*, pages 18–23. Springer.

Tscherning, C. C. and Rapp, R. H. (1974). Closed covariance expressions for gravity anomalies, geoid undulations, and deflections of the vertical implied by anomaly degree variance models. *Scientific Interim Report Ohio State Univ., Columbus. Dept. of Geodetic Science.*

Tziavos, I., Andritsanos, V., Forsberg, R., and Olesen, A. (2005). Numerical investigation of downward continuation methods for airborne gravity data. In *Gravity, Geoid and Space Missions*, pages 119–124. Springer.

VALLIANT, H. (1991). The la coste and romberg air/seagravity meter: An overview.

Wang, X.-T., Xia, Z.-R., Shi, P., and Sun, Z.-M. (2004). A comparison of different downward continuation methods for airborne gravity data. *Chinese journal of Geophysics*, 47(6):1143–1149.

Wang, Y., Becker, C., Mader, G., Martin, D., Li, X., Jiang, T., Breidenbach, S., Geoghegan, C., Winester, D., Guillaume, S., et al. (2017). The geoid slope validation survey 2014 and grav-d airborne gravity enhanced geoid comparison results in iowa. *Journal of Geodesy*, 91(10):1261–1276.

Ward, A. (2004). Gravity recovery and climate experiment (grace). *NASA, March*, 30.

APPENDICES

APPENDIX A : Principle of airborne gravimetry
APPENDIX B : The computed covariance values of Test-1, Test-2, Test-3, and Test-4
APPENDIX C : Job file description, directory structure and the scheme of quasi-geoid computations, and flowchart of the quasi-geoid computation from residual gravity anomalies for airborne, surface and combined data

APPENDIX A

Basic principle of airborne gravimetry relies on the acceleration measurements which happens due to gravitational attraction ($\underline{g}$) and some forces (f) caused by vehicle movement. The force that accelerometer measure is

$$f = \underline{g} - \underline{\ddot{r}} \tag{A.1}$$

where $\underline{\ddot{r}}$ is the position vector of the aircraft which is known from kinematic GPS observations. Therefore, one can find the gravitational acceleration. However, the given equation holds for an inertial reference system which is neither rotating nor accelerating. In a rotating system as in local coordinate system (East, North, Up), Equation **A.1** becomes

$$\underline{f} = \underline{g} - \ddot{r} - \underline{\Omega} \times \underline{\Omega} \times \underline{r} + 2\underline{\Omega} \times \underline{\dot{r}} + \underline{\dot{\Omega}} \times \underline{r} \tag{A.2}$$

where $\underline{\Omega}$ is the rotation vector. First correction term ($\underline{\Omega} \times \underline{\Omega} \times \underline{r}$) represents the centrifugal force, second one ($2\underline{\Omega} \times \underline{\dot{r}}$) is the Coriolis force which is an inertial force that acts on a moving object within a frame that rotates with respect to an inertial frame. And the last correction ($\underline{\dot{\Omega}} \times \underline{r}$) is Euler term. These equations are based on the assumption of ($\underline{g}$) is known, position and the velocity are found from the measurements by ring laser gyros. The general equation to obtain the vertical component, i.e. gravity vector, from airborne gravimetry, Equation **A.2** becomes

$$g_D = a_D - \dot{v}_U - \left(\dot{\lambda} + 2\omega_{\text{ie}}\right) \cos\varphi \cdot v_\varepsilon - \dot{\varphi} \cdot v_N \tag{A.3}$$

where φ and λ are latitude and longitude, $v_{N,E,U}$ represents the velocity vector, respectively, ω the sideral earth rate. In here, the Euler term is neglected due to the fact that rotation rate is assumed to be constant. Later, the effect of the centrifugal force is considered in normal gravity.

In another way, the observed gravity value (g_D) can be expressed as the sum of gravity anomaly (Δg) and normal gravity (γ) as in

$$g_D = \Delta g + \gamma \tag{A.4}$$

Since gravity is considered to be a value obtained from a relative measurement, the fundamental equation to express the gravity becomes

$$\Delta g = a - h'' - \delta g_{\text{eot}} - \delta g_{\text{tilt}} - y_0 + g_0 - \gamma_0 + 0.3086(h - N) \tag{A.5}$$

where a is the acceleration that is measured along the vertical, h'' is GPS derived vertical acceleration, a_0 is the zero level of the gravimeter (e.g. airport base reading), g_0 is the gravity value at the airport reference, γ_0 is the normal gravity at sea level. In a normal case, the vertical acceleration measurement is carried out on a platform which is gyro-stabilized. However, this situation changes when it is done on a moving platform such as airborne. There will be some tilts in a, which can be corrected by the term δg_{tilt} as in

$$\delta g_{\text{tilt}} = \frac{a^2 - q^2}{2g} \tag{A.6}$$

where q is true horizontal acceleration. Additionally, the measurements are held over a curved rotating surface i.e. Earth, Eotvos correction (δg_{eot}) is a necessary term. This term is expressed by Earth rotation rate, north and east velocity components as

$$\delta g_{\text{eot}} = -2\omega \cos\varphi v_E - \left(v_N^2 + v_E^2\right)/R \tag{A.7}$$

These correction terms are important in order to have a bias-free airborne gravimetry data. In addition to that, cross-over adjustment can be performed to eliminate residual, unmodeled error. There are also other type of errors such as internal measurement and calibration errors which changes according to used instrument and can be computed in real time (VALLIANT, 1991). This situation is slightly reduced by the modern INS (Inertial Navigation System) - grade accelerometers. These new type of instruments provide a good quality observation due to enhanced INS-style processing and sensor performance (Studinger et al., 2008). Even though all of the correction terms are included, the vertical acceleration both measured and derived from GPS are highly effected by the airborne dynamics such as turbulence, autopilot performance and of course the aircraft type (Forsberg and Olesen, 2010). Therefore, all of the terms needs to be filtered.

APPENDIX B

Table B.1 : The computed covariance values of Test-1, Test-2, Test-3, and Test-4 that is mentioned in Section 4.1 for the given spherical distance (ψ). [unit: mGal^2]

ψ (degree)	Test-1	Test-2	Test-3	Test-4
0.000	28.8022	28.8023	41.1454	35.0218
0.025	26.3041	26.3042	37.5766	31.6318
0.050	20.2902	20.2903	28.9851	23.5266
0.075	13.4288	13.4289	19.1829	14.4206
0.100	7.4114	7.4115	10.5865	6.6507
0.125	2.7859	2.7860	3.9785	0.9455
0.150	-0.4736	-0.4735	-0.6779	-2.7758
0.175	-2.5794	-2.5794	-3.6862	-4.8580
0.200	-3.7709	-3.7709	-5.3883	-5.6841
0.225	-4.2644	-4.2644	-6.0932	-5.6022
0.250	-4.2432	-4.2432	-6.0627	-4.9088
0.275	-3.8599	-3.8599	-5.5150	-3.8491
0.300	-3.2403	-3.2403	-4.6298	-2.6212
0.325	-2.4879	-2.4879	-3.5547	-1.3805
0.350	-1.6862	-1.6862	-2.4094	-0.2435
0.375	-0.9016	-0.9016	-1.2883	0.7088
0.400	-0.1845	-0.1845	-0.2637	1.4274
0.425	0.4289	0.4290	0.6127	1.8913
0.450	0.9154	0.9154	1.3076	2.1035
0.475	1.2631	1.2631	1.8045	2.0864
0.500	1.4706	1.4706	2.1009	1.8768
0.525	1.5447	1.5447	2.2068	1.5215
0.550	1.4994	1.4994	2.1421	1.0718
0.575	1.3537	1.3537	1.9340	0.5795
0.600	1.1302	1.1302	1.6147	0.0931
0.625	0.8532	0.8532	1.2189	-0.3458
0.650	0.5474	0.5474	0.7820	-0.7046
0.675	0.2361	0.2361	0.3373	-0.9609
0.700	-0.0594	-0.0594	-0.0848	-1.1037
0.725	-0.3213	-0.3213	-0.4590	-1.1325

APPENDIX C

Job file description for EMPCOV:

- Step for covariance evaluation; num. of emp cov values to be computed, 1, F = plot of cov, T = output of cov in a file, T = subtract mean value from data
- Name of the output file which holds the empirical covariance values
- Total number of the data points inside the input data, input data in free format = 9, T = latitude in the first record, 3 = coordinates are given in degree, data type (3 for Δg), 0 = no other data, 1, F = all data must be considered
- 2 = two data are in each record, 2 = use the second one, 0 = no other data are in each record
- Name of the input file
- T = no other input files

Job file description for COVFIT:

- Fit (4) or not fit (1) to the($\Delta g = 3$) empirical covariance, F, F, T, F
- Model of degree variance
- Depth of Bjerhammar sphere in km (R_B), variance of the signal (C_0), error degree varinances up to degree N
- Error degree variance from file = 0, minimum degree, scale factor of the error degree variances
- File containing error degree variances
- Additive coefficient for error degree var
- Number of sample, step for covariance evaluation, azimuth
- Functional ($\Delta g = 3$), functional ($\Delta g = 3$), mean height of those functionals

Job file description for GEOCOLIGS:

- Do the computation (itest = 0)
- Functional of the observation ($\Delta g = 3$), consider the data at their height (0)
- Input data
- File format of the input data

- Variance of the data ($mGal^2$), depth of Bjerhammar sphere (in m), covariance model, error degree up to N, noise variance ($mGal^2$), F, T = error degree variances are non-zero
- Functional to be predicted, prediction is point-wise
- File containing prediction points
- File format
- Output file holding the predictions
- File format
- Error degree variance from file = 0, minimum degree, scale factor of the error degree variances
- File containing error degree variances

Table C.1 : Directory structure followed in the quasi-geoid computations

Program	Input	Data description	Explanation
EMPCOV	filtered_airborneFAA2.dwc	Downward continued airborne residual gravity anomalies	Compute emp.cov. separately, then fit the model cov. to emp.cov
	Terrestrial_residuals.txt	Residual surface gravity anomalies	
COVFIT	ggm.edv	Error degree variance file	
GEOCOLIGS	filtered_airborneFAA2.dwc	Downward continued airborne residual gravity anomalies	Computation of airborne only quasi-geoid model
	ha_airborne.pred	File contains prediction points	
	ggm.edv	Error degree variance file	
	ha_airborne.est	File contains the estimations	
GEOCOLIGS	Terrestrial_residuals.txt	Residual surface gravity anomalies	Computation of terrestrial only quasi-geoid model
	ha_terr.pred	File contains prediction points	
	ggm.edv	Error degree variance file	
	ha_terr.est	File contains the estimations	
GEOCOLIGS	terr_air.res	Residual surface and downward continued gravity anomalies	Combining the surface and downward continued airborne gravity anomalies
	dg_comb.pred	File contains prediction points	
	ggm.edv	Error degree variance file	
	dg_comb.est	File contains the estimations	
GEOCOLIGS	dg_comb.est	Combined grid of residual gravity anomalies	Computation of combined quasi-geoid model
	ha_comb.pred	File contains prediction points	
	ggm.edv	Error degree variance file	
	ha_comb.est	File contains the estimations	
res_valid.m	ha_*.est	Files contain the estimated height anomalies for all solutions	Restore ζ_{Res} computed at GPS/Lev points convert ζ to N in order to validate over sparse GPS/Lev points

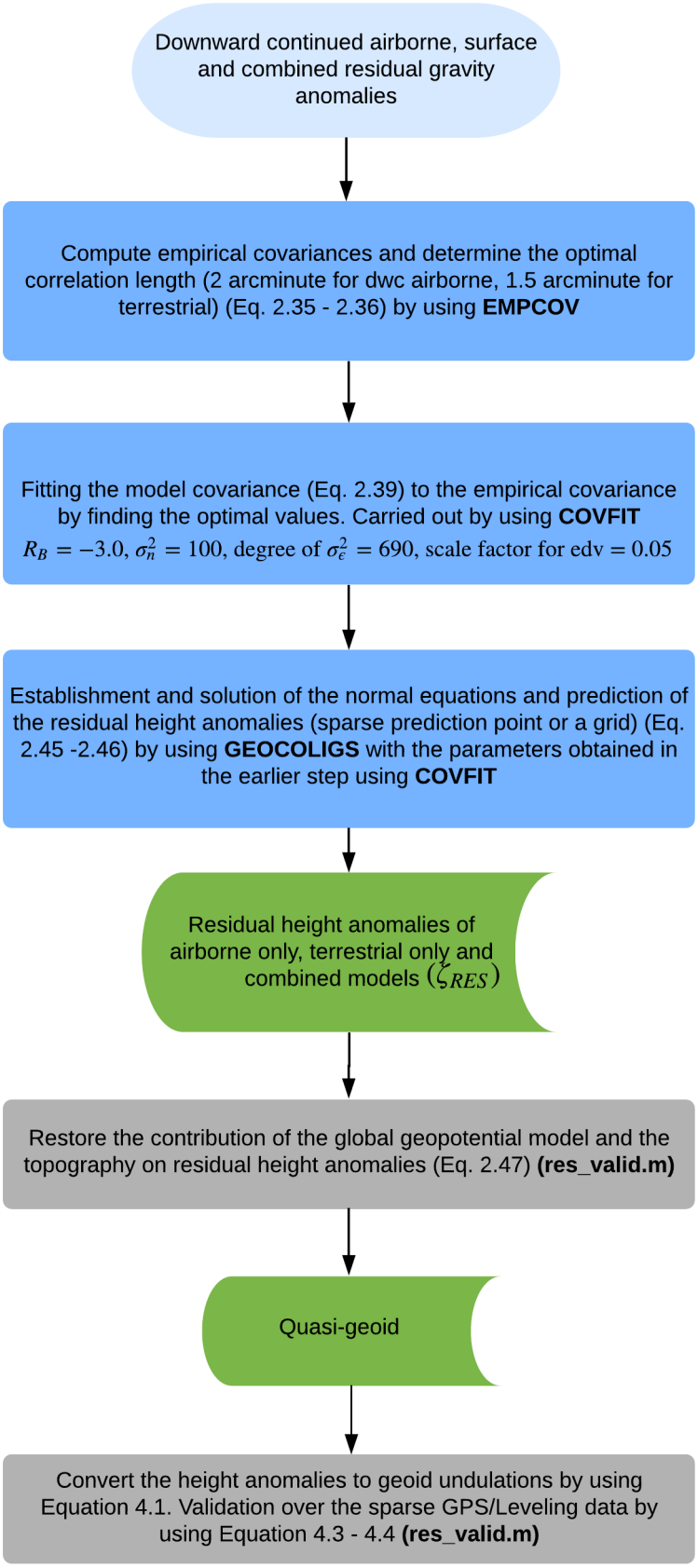

Figure C.1 : Quasi-geoid computation from residual gravity anomalies for airborne, surface and combined data.

CURRICULUM VITAE

Name Surname: Öykü Koç

Place and Date of Birth: Beyoğlu, Istanbul - 19/11/1995

E-Mail: kocoy@itu.edu.tr

EDUCATION:

- **B.Sc.:** 2018, Istanbul Technical University, Faculty of Civil Engineering, Geomatics Engineering Department
- **M.Sc.:** 2020, Istanbul Technical University, Graduate School of Science, Engineering and Technology, Geomatics Engineering Programme

PROFESSIONAL EXPERIENCE AND REWARDS:

- 09-12/2019 Visiting student, DICA, Politecnico di Milano, Milano/Italy.
- 03/2018 Best Poster Award, Geo-information for Disaster Management 2018 Annual Conference (Gi4DM 2018).
- 07-09/2017 Intern, IGS-ISTA Observation and Geodetic Laboratory,Istanbul Technical University, Istanbul/Turkey
- 07-08/2016 Intern, ODAKENT Env. Inf. Inc, Istanbul/Turkey.

PUBLICATIONS, PRESENTATIONS AND PATENTS ON THE THESIS:

- Grigoriadis, V. N., Vergos, G. S., Barzaghi, R., Carrion, D., and Koç, O. (2020). Collocation and FFT-based geoid estimation within the colorado 1 cm geoid experiment. *Journal of Geodesy*, Under Review
- Koc, O., Erol, S., Isk, M.S. Erol, B.(2019) Contribution of Cryosat 2 SAR/SARin Data to Local Vertical Datum Validation and Height System Unification in Turkey, IUGG General Assembly 2019
- Koc, O., Erol, S., Isk, M.S. Erol, B.(2018) Validation of Mediterranean Sea MSS and Marine Geoid using Recent Global and Regional Models, Local Tide Gauge and Coastal Altimetry Products, GGHS 2018
- Akyurek, D., Koc, O., Akbaba, E. M. Sunar, F.(2018) Land use/land cover change detection using multitemporal satellite dataset: a case study in Istanbul new airport, Int. Arch. Photogramm. Remote Sens. Spatial Inf. Sci., Gi4DM 2018, ISPRS